PCCP

ROYAL SOCIETY OF CHEMISTRY

PAPER

View Article Online
View Journal | View Issue

Cite this: *Phys. Chem. Chem. Phys.*, 2020, **22**, 24744

Hydrophobic functional liquids based on trioctylphosphine oxide (TOPO) and carboxylic acids†

Emily L. Byrne, Ruairi O'Donnell, Mark Gilmore, Nancy Artioli, John D. Holbrey * and Małgorzata Swadźba-Kwaśny *

Received 13th May 2020,
Accepted 5th October 2020

DOI: 10.1039/d0cp02605k

rsc.li/pccp

Trioctylphosphine oxide (TOPO) is a hydrophobic extracting agent used in a number of commercially important separations of valuable solutes from aqueous streams (with examples ranging from lanthanides, through gallium, to carboxylic acids). TOPO is traditionally used as a solute in kerosene, its extraction efficiency limited by its solubility in the organic diluents. In this work, eighteen hydrogen bond donors (HBDs) were screened for their capacity to liquefy TOPO, employing strategies used to design deep eutectic solvents (DES). The selected HBDs were all useful in separations and were designed to formulate solvent-free, hydrophobic, bi-functional liquid extracting agents. Some TOPO:HBD mixtures yielded hydrophobic liquids that offer potential to be extremely efficient extractants, incorporating high intrinsic concentrations of TOPO. Following this initial screening, two systems: TOPO:malonic acid and TOPO:levulinic acid, were selected for detailed physico-chemical characterisation across their complete compositional ranges. Phase diagrams, thermal stabilities and the mechanism of thermal decomposition are reported, along with densities and insights from ^{31}P NMR spectroscopic studies. The work was concluded with a proof-of-concept demonstration of the use of the TOPO:malonic acid (2 : 1 mol ratio) mixture for the extraction of gallium from acidic chloride feedstock (simulated pre-digestate of zinc leach residue). The loading capacity of the TOPO:malonic acid extractant was three orders of magnitude greater than that of the literature benchmark, encouraging further application-oriented studies.

Introduction

The phrase deep eutectic solvent (DES) describes a eutectic mixture with significant melting point depression relative to that of its individual components (below thermodynamic lines).[1] However, it should be noted that many authors adopt a much broader definition, using it to describe any two-component mixture that is liquid at room temperature at a given molar ratio. DES are traditionally comprised of a salt with a bulky organic cation and a much smaller Lewis-basic anion acting as a hydrogen bond acceptor (HBA) and a hydrogen bond donor (HBD).[2–6] First reported in 2003, archetypal examples of DESs pair choline chloride with alcohols, carboxylic acids or amides (*e.g.* urea) as HBD species.[5] Perceived as environmentally benign and inexpensive types of (or alternatives to) ionic liquids, DESs have gained popularity as solvents for protein extraction,[7] metal electrodeposition,[2,4] organic synthesis[2,4] and drug solubilisation.[2] There has been a recent publication concerning metal recovery using these choline chloride eutectic systems;[8] however, the applications that remained largely unexplored were aqueous biphasic extractions and other uses demanding hydrophobic liquids. Due to the abundance of hydrogen bonding and coulombic interactions,[9–16] all early DESs were completely miscible with water.

A breakthrough came in 2015, with two parallel publications describing hydrophobic eutectics, each representing a different approach. Kroon and co-workers formulated a hydrophobic eutectic by the introduction of long alkyl chains to traditional motifs of an organic halide salt combined with a carboxylic acid, combining decanoic acid with long-chain quaternary ammonium salts.[17] Marrucho and co-workers took a naturally-occurring and intrinsically hydrophobic component (a terpene) and combined this with organic acids (*e.g.* pyruvic or lauric acid) to form non-ionic eutectics based on menthol.[18] Both families of hydrophobic eutectics have been explored as solvents for extraction and partitioning from aqueous sources. A range of long chain quaternary ammonium salts combined with long chain carboxylic acids or alcohols and menthol-derived hydrophobic eutectics

The QUILL Research Centre, School of Chemistry and Chemical Engineering, Queen's University Belfast, David Keir Building, Stranmillis Road, Belfast, BT9 5AG, UK. E-mail: m.swadzba-kwasny@qub.ac.uk, j.holbrey@qub.ac.uk

† Electronic supplementary information (ESI) available: NMR spectra, DSC and TGA thermograms and tabulated data. See DOI: 10.1039/d0cp02605k

have been examined as extracting phases for organic molecules,[19,20,30–35] metal ions,[21–23,36] pesticides,[24] and biomolecules[18,25] from aqueous solution, as well as bioactive compounds from biomass.[26–30]

A major advantage of the menthol-based non-ionic hydrophobic eutectics is their relatively low viscosity (12–43 mPa s at 25 °C)[18] compared to those of the ionic hydrophobic eutectics from Kroon and co-workers (173–783 mPa s at 25 °C), which can be a major advantage in application to liquid–liquid extraction.[17]

In our group, there is a long-standing interest in the use of trioctylphosphine oxide (TOPO) in the formulation of functional liquids. TOPO is an abundantly available, moderately basic, hydrophobic phosphine oxide. It is a good hydrogen bond acceptor and a good ligand, finding numerous applications as an extractant for metals (particularly lanthanides),[31,32] organic acids,[33–36] and phenolic species[37–40] from aqueous streams. Phosphine oxides are used industrially in the TRUEX and TRPO processes for removing actinides (including uranium) from radioactive waste.[41,42]

Under ambient conditions TOPO is a solid, therefore, in order to be used in extraction it needs to be dissolved in a hydrophobic solvent; typically kerosene. However, the relatively low solubility of TOPO in apolar organic solvents as extracting phases is a major drawback in its industrial use, limiting extraction due to low TOPO concentrations. To circumvent this, the liquid Cyanex 293 (a mixture of C_6–C_8 phosphine oxides) was formulated; however, this utilises more expensive phosphine oxides as liquifying components, significantly increasing the cost of the extraction medium.[40] Furthermore, shorter-chain phosphine oxide components are more prone to leaching to aqueous phases.

In our previous work, TOPO has been used as a ligand to formulate Lewis acidic liquid coordination complexes (LCCs), the long chains enhancing liquid formation and increasing the hydrolytic stability of the Lewis acidic catalysts.[43–46] This work inspired research into the potential to incorporate TOPO as a component of a eutectic in 2018, which would have an intrinsically high concentration of this powerful and versatile extracting agent. A similar approach was taken by Meuldijk and co-workers around the same time to extract volatile fatty acids from aqueous feedstock.[47] In the work from our group, however, a TOPO:phenol eutectic was reported and successfully used to extract uranyl from a model waste stream.[48] Phenol was used to liquefy TOPO, being much cheaper than phosphine oxides, and already known as a strong hydrogen bond donor to TOPO.[37–40] However, considering the functionality of the TOPO:phenol eutectics in extraction, phenol was merely a spectator and, in addition, raises concerns about potential contamination of the treated aqueous stream with phenol.

In this work, we report bifunctional TOPO-based eutectics, characterised by very high TOPO concentrations, with the potential to fine-tune the extraction selectivity by selecting an appropriate HBD. In addition, they are of low environmental concern due to the benign nature of the screened components. A range of mixtures was screened for the formation of ambient-temperature liquids, followed by an in-depth study of the thermal stability and phase behaviour of two systems, and a proof-of-concept demonstration of the extracting ability of one of these mixtures. We believe that this fundamental study will underpin the development of a new and versatile family of hydrophobic extractants, benefitting from synergies in the extracting ability of both components, low cost, very high partition coefficients and no requirement for organic solvents.

Experimental

Materials

TOPO (>97%) was kindly provided by Solvay. Hydrochloric acid (37%), benzene, malonic acid (99%), palmitic acid (>99%), D-(+)-cellobiose (98%), catechol (>99%), gentisic acid (98%), 2,6-xylenol (99%), 4-tertbutylphenol (99%), levulinic acid (98%), stearic acid (>99%), (±)-α-lipoic acid (>98%), resorcinol (99%), gallic acid (98%), pyrogallol (99%), 8-hydroxyquinoline-2-carboxylic acid (98%) and (+)-sodium L-ascorbate (98%) were purchased from Sigma Aldrich. Gallium(III) chloride (99.999%) was purchased from Alfa Aesar and salicylic acid (98%) was purchased from Fluorochem. For screening studies on eutectic formation, all chemicals were used as received, with the exception of catechol, which was recrystallised from hot toluene followed by sublimation on a Schlenk line (80 °C, 10^{-2} mbar, 24 h) before use. For thermophysical characterisation studies, all chemicals were dried and stored in a glove box until use (MBraun Lab Master dp, <0.6 ppm O_2 and H_2O).

TOPO was dried by heating under reduced pressure on a Schlenk line (60 °C, 10^{-2} mbar, 24 h). Levulinic acid was dried by heating under reduced pressure on a Schlenk line (40 °C, 10^{-2} mbar, 48 h). They were both stored in a glove box as white solids. Malonic acid was dissolved in dry ethyl acetate and dried with magnesium sulfate. The suspension was filtered at 70 °C and the filtrate was placed on a rotary evaporator to remove the solvent (60 °C), dried on a Schlenk line (60 °C, 10^{-2} mbar, 24 h) and stored in a glove box.

Preparation of mixtures

In the screening experiments, TOPO was combined directly (solventless) with the hydrogen bond donors shown in Table 1 at given molar ratios. The mixtures were heated to 60 °C with stirring for 2 hours, or until homogeneous liquids formed.

For detailed thermophysical characterisation, TOPO:malonic acid and TOPO:levulinic acid mixtures were prepared (solventless) by combining mole fractions of each component together across the compositional range (χ_{TOPO} = 0.1–0.9) under an inert atmosphere, with accuracy to ±0.0003 g, and subsequently heating the mixture to 60 °C with stirring for 2 hours or until a homogeneous liquid was obtained. The samples typically formed white solids, colourless liquids or partially solid/liquid mixtures at room temperature after preparation depending on the mole ratio of the components used. Homogeneous TOPO:malonic acid liquid samples were obtained between χ_{TOPO} = 0.55

Table 1 Mixtures of TOPO with hydrogen bond donors (HBDs) and their physical appearance at ambient temperature and at 8.5 °C. All HBDs used were solid at ambient temperature. $T_{m\ (TOPO)}$ = 52 °C

HBD	Potential use	χ_{TOPO}	Room temperature	In the fridge (8.5 °C)
Palmitic acid T_m = 63 °C[49]	Carboxylic extraction from fermentation broth	0.40	White gel-like material	—
		0.50	White gel-like material	—
		0.60	White gel-like material	—
		0.67	White solid	—
Stearic acid T_m = 70 °C[49]	Carboxylic extraction from fermentation broth	0.50	White solid	White solid
Cellobiose T_m = 224 °C[50]	Carboxylic extraction from fermentation broth/ nanoparticle synthesis	0.50	White solid	—
		0.67	White solid	—
		0.88	White solid	—
Pyrogallol[a] T_m = 133 °C[51]	Nanoparticle synthesis/ phenolics extraction	0.50	Colourless liquid with solid ppt	—
		0.67	Colourless liquid	Gel-like material
		0.75	Waxy gel-like material	—
Resorcinol[a] T_m = 109 °C[52]	Nanoparticle synthesis/ phenolics extraction	0.50	Colourless liquid	Colourless liquid
		0.67	Colourless liquid	Colourless liquid
Gallic acid[a] T_m = 258 °C[53]	Nanoparticle synthesis/ phenolics extraction	0.50	Colourless liquid with solid ppt	Gel-like material
		0.67	Colourless liquid	Colourless liquid
		0.75	Gel-like material	Gel-like material
4-Tertbutylphenol T_m = 99 °C[54]	Phenolics extraction	0.50	Colourless liquid	Colourless liquid
2,6-Xylenol T_m = 44 °C[55]	Phenolics extraction	0.50	Colourless liquid	Colourless liquid
Catechol T_m = 104 °C[56]	Nanoparticle synthesis/ phenolics extraction	0.40	Colourless liquid	Colourless liquid
		0.50		

Table 1 (*continued*)

HBD	Potential use	χ_{TOPO}	Room temperature	In the fridge (8.5 °C)
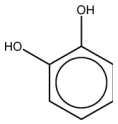			Colourless liquid	Colourless liquid
		0.60	Colourless liquid	Colourless liquid
		0.67	Gel-like material	—
4-Methoxybenzoic acid T_m = 184 °C[57] 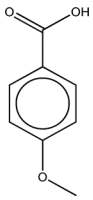	Carboxylic extraction from fermentation broth	0.50	Colourless liquid with solid ppt	White solid
Lipoic acid T_m = 61 °C[58] 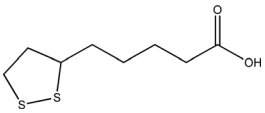	Carboxylic extraction from fermentation broth	0.50	Yellow liquid	Yellow liquid
Gentisic acid T_m = 205 °C[59] 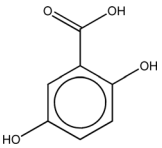	Phenolics extraction	0.50	Yellow liquid with solid ppt	Mostly solid with some liquid
		0.67	Yellow liquid	Yellow liquid
		0.75	Yellow solid	Yellow, circular, beady solid
Malonic acid T_m = 137 °C (lit. 136 °C)[60] 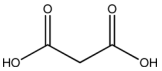	Gallium extraction	0.67	Colourless liquid	—
Levulinic acid T_m = 32 °C (lit. 32 °C)[61] 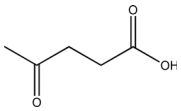	Carboxylic extraction from fermentation broth	0.50	Colourless liquid	Colourless liquid
Salicylic acid T_m = 158 °C[62] 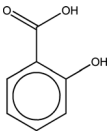	Gallium extraction/ phenolics extraction	0.50	Colourless liquid	Colourless liquid
		0.67	White solid	—
8-Hydroxyquinoline-2-carboxylic acid T_m = 216 °C[63] 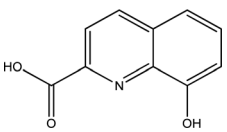	Gallium extraction	0.50	Yellow liquid	—
		0.67	Yellow gel-like material	—
		0.75	Yellow gel-like material	—
Diphenylacetic acid T_m = 148 °C[64] 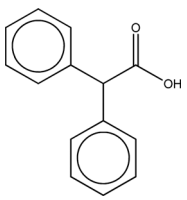	Gallium extraction	0.50	Colourless liquid	Colourless liquid

[a] Samples turned increasingly pink to brown after a few hours/days; ppt = precipitate.

and 0.67 at ambient temperature. χ_{TOPO} = 0.50 was a mostly liquid sample with trace solid at ambient temperature. Homogeneous TOPO:levulinic acid liquid mixtures were obtained between χ_{TOPO} = 0.30 and 0.50 at ambient temperature. χ_{TOPO} = 0.10–0.20 were mostly liquid samples with a small amount of solid at ambient temperature. The samples were stored in a glove box until use.

Thermogravimetric analysis

The thermal stability and decomposition routes were examined by thermogravimetric analysis (TGA) using a TA Instruments Q5000 TGA. Tzero aluminium pans and Tzero aluminium hermetic lids were used and the samples prepared within a dry argon atmosphere within a glove box. Dynamic heating regimes were applied at 10 °C min^{-1} from room temperature to 400 °C to determine the onset of thermal decomposition, T_d (onset), for each sample across the compositional range. T_d (onset) was determined by visual determination of the initial deviation of the derivative of the TG curve (DTG curve) from its baseline.

Isothermal regimes were used to determine the initial rate of decomposition and/or mass loss corresponding to a particular component of the mixture. The samples were rapidly heated (50 °C min^{-1}) to determined temperatures to limit the initial decomposition and then the mass loss was monitored under isothermal control. The isothermal temperatures selected were within the range of the first step of decomposition, at a low enough temperature to ensure that stage 2 decomposition does not occur, but high enough for decomposition to proceed at a reasonable rate. The samples were held isothermally for 22 h. For the TOPO:malonic acid mixtures, the sample was examined at 90 °C, and for the TOPO:levulinic acid mixtures, at 90 and 140 °C.

Analysis of the decomposition products

TOPO:malonic and levulinic acid mixtures (χ_{TOPO} = 0.33) were prepared in a 2-necked round bottomed flask with vacuum taps attached within a glove box, as outlined above, and stored until use. This was removed from the glove box and connected to gas rig apparatus equipped with a gas chromatography-mass spectrometer (GC-MS) and purged with argon before heating. TOPO:malonic acid samples were held isothermally at 90 °C and TOPO:levulinic acid samples were held isothermally at 90, 125 and 140 °C to achieve a reasonable decomposition rate. *In situ* evolved gas analysis using GC-MS was used to evaluate the volatile thermal decomposition products. The levels of H_2, H_2O, CO_2, CO and O_2 gases were monitored throughout. Analysis of the liquid phase was performed using NMR (see below).

NMR spectroscopy

Neat liquid TOPO:malonic acid (χ_{TOPO} = 0.50–0.67) and TOPO:levulinic acid (χ_{TOPO} = 0.10–0.20) were examined by NMR spectroscopy. The samples were prepared in a glove box under a dry argon atmosphere and transferred directly to NMR. ^{31}P NMR spectra were recorded on a Bruker Avance DPX 400 MHz spectrometer at 162 MHz with a sealed D_3PO_4 capillary added to supply an external lock, referencing the spectra to D_3PO_4 (δ^{31}P = 0 ppm). For ^{1}H (400 MHz) and ^{13}C (101 MHz) NMR measurements, a sealed d_6-DMSO capillary was used to supply the external lock and reference.

To determine the species formed in the liquid phase as a result of decomposition, ^{13}C NMR measurements were performed on a 400 MHz Bruker Avance DPX spectrometer at 101 MHz. TOPO:malonic acid samples were dissolved in d_6-acetone as they were not homogeneous liquids at χ_{TOPO} = 0.33 at ambient temperature. TOPO:levulinic acid samples were run neat with a d_6-DMSO capillary as a reference.

Differential scanning calorimetry

Phase diagrams for TOPO based functional liquids where TOPO acts as the hydrogen bond acceptor with malonic acid or levulinic acid as hydrogen bond donors were constructed using differential scanning calorimetry (DSC) and visual observation of the melting point using a solid liquid cell (SLC) apparatus.

The upper thermal stability limit of each mixture was first determined using TGA and then DSC measurements were performed using a TA Instruments Q2000 DSC with an RCS 90 cooling system attached. Tzero aluminium pans were filled with the sample (typically *ca.* 8 mg) and sealed with Tzero hermetic lids within a glove box under a dry argon atmosphere before being transferred outside the glovebox to the DSC. DSC measurements were repeated in 3 cycle runs with heating and cooling occurring at 2 °C min^{-1} between −90 and 80 °C or below. In all cases, the samples were run below their upper thermal stability limit before thermal decomposition occurred. Between the heating and cooling cycles, the samples were held isothermally for 5 minutes to allow the sample to thermally equilibrate before the subsequent cycle began. The maxima of all phase transitions were recorded.

Visual melting point determination

The visual melting point was determined using a solid–liquid cell apparatus. The phase observed as a function of temperature was recorded for samples (3 cm^3) pre-loaded into a sealed Pyrex glass solid liquid cell containing a stirrer bar within the glove box. The samples were removed from the glove box and placed in a thermostated water or ethanol bath with a thermocouple immersed in the bath, secured around the exterior of the solid liquid cell, and the temperature was allowed to equilibrate for 30 minutes (1 °C increments near phase transitions). The stirring rate was fixed at 400 rpm. Temperatures above 0.0 °C were controlled using a Julabo circulating bath and temperatures below 0.0 °C, down to −60.0 °C, were achieved with the addition of liquid nitrogen to the surrounding ethanol bath. When the liquidus point had not been reached above 68.0–80.0 °C, a silicon oil bath was used and the temperature controlled by the Pt 1000 temperature sensor on a Heidolph Hei-Tec heating plate. In all cases, an Omega type K (5SC) thermocouple with an HH802U thermocouple thermometer was used to determine the temperature. In the solid–liquid cell measurements there were two points of interest for the phase

change of the crystalline mixtures: the temperature at which the magnetic stirrer bar started to move within the cell and the temperature at which a clear homogeneous liquid was formed on heating. Due to the liquidus point for a number of TOPO: malonic acid samples being above their thermal decomposition temperature (*i.e.* for χ_{TOPO} = 0.00–0.33), clear yellow liquids were obtained at the liquidus point. In non-crystalline glassy samples (*i.e* χ_{TOPO} = 0.60 for TOPO:malonic acid and χ_{TOPO} = 0.40 for TOPO:levulinic acid), the phase change was observed during passive warming to ambient temperature following previous cooling using liquid nitrogen addition to an ethanol bath as the temperature at which stirrer bar motion could be detected within the solid liquid cell. In this case, the average heating rates were 1–2 °C min^{-1}. All samples were repeated twice or more.

Density

Density measurements for homogeneous liquid TOPO:malonic acid mixtures between χ_{TOPO} = 0.55 and 0.67 and TOPO: levulinic acid mixtures between χ_{TOPO} = 0.30 and 0.50 were performed. The liquid phase of TOPO:malonic acid at χ_{TOPO} = 0.50 and TOPO:levulinic acid mixtures between χ_{TOPO} = 0.10 and 0.20 was also sampled and measured. Density measurements were performed on an Anton Paar DMA 4500 M density meter over a temperature range of 20–50 °C in increments of 5 °C. The samples were transferred to a syringe under a dry argon atmosphere and kept in a glove box until the density measurements were performed.

Leaching study

Two TOPO:malonic acid liquid samples at the extremities of the homogeneous liquid range (*i.e.* χ_{TOPO} = 0.55 and 0.67) were selected for the study. Two samples of each composition were prepared and combined in a shaking tube with an equi-volume of deionised water (polished to 18.2 MΩ cm^{-1}) or a 6 M HCl aqueous phase. These mixtures were shaken on a Stuart scientific flask shaker SF1 (20 min, ambient temperature) and subsequently centrifuged to achieve good phase separation. The malonic acid concentration in the aqueous phase post-contact with deionised water was determined by both FT-IR and the total organic carbon content (TOC). An Agilent Technologies Cary 630 FT-IR spectrometer was used to record FT-IR spectra. A Shimadzu TOC-L analyser was used to quantify the total organic carbon content. For FT-IR calculations, a calibration curve of the malonic acid concentration in deionised water (3.25–90.00 g L^{-1}) was first generated by plotting the aqueous malonic acid concentration against transmittance (Fig. S12, ESI†) and fitting to the linear equation ($y = mx + c$, R^2 = 0.9981). The R^2 = 0.9519 derived for the 6 M HCl calibration curve was found to be unsatisfactory, and therefore leaching of malonic acid into 6 M HCl was quantified by TOC.

For TOC calculations, the amount of carbon corresponding to malonic acid (g L^{-1}) in the aqueous phase was calculated using eqn (1). [MA] is the concentration of malonic acid (g L^{-1}), TOC_{raw} (ppm) is the raw concentration of carbon in the sample, TOC_w (ppm) is the concentration of carbon in a blank water sample, d is the dilution factor, RMM_{MA} (g mol^{-1}) is the relative molecular mass of malonic acid and $RMM_{total\ carbon}$ (g mol^{-1}) is the relative molecular mass of the total number of carbons present in the sample.

$$[MA] = \frac{TOC_{raw} - TOC_w \cdot d \cdot RMM_{MA}}{(1000) \cdot RMM_{totalcarbon}} \quad (1)$$

Typical extraction procedure

The de-ionised water used to make HCl stock solutions was collected from a Barnsted deionisation system, polished to 18.2 MΩ cm^{-1}. HCl stock solutions were prepared in volumetric flasks at molar concentrations between 1 and 8 M HCl. Acidic chloride stock solutions of gallium were prepared by weighing gallium(III) chloride into a 2-necked round bottom flask in a dry, argon environment within a glove box. This was then sealed and transferred to Schlenk line apparatus where a steady flow of argon was flowed over the flask and the HCl stock added dropwise with ice bath cooling. Following dilution with de-ionised water, the gallium content in the aqueous phase was determined by inductively coupled plasma (ICP) using an Agilent Technologies 5100 ICP-OES spectrometer.

For the partitioning studies, a given volume of extractant (*i.e.* χ_{TOPO} = 0.67 TOPO:malonic acid) was added to a centrifuge tube, pre-equilibrated with an equivolume of HCl stock solution with a concentration corresponding to that of the stock used for the extraction of gallium, and then contacted with an equivolume of acidic chloride gallium stock (unless stated). When replicating the literature benchmark at 6 M HCl,[31] 0.004 M TOPO diluted in benzene was prepared as the extractant phase. This extractant phase was first pre-equilibrated by contact with an equivolume of HCl stock solution with a concentration corresponding to that of the stock used for the extraction of gallium. It was then contacted with an equivolume of acidic chloride gallium stock (0.00568 M $GaCl_3$).

Both the pre-contact and extraction times in all cases were 10 min and the biphasic samples were mixed using a mechanical shaker (Burrell, model 75). After pre-contact and extraction, the samples were centrifuged, and the aqueous phase separated from the extracting phase. The gallium content present in the aqueous phase post extraction was determined by ICP-OES following dilution (if required).

The gallium extraction efficiency (%) was calculated using eqn (2) from the difference in $[Ga]_{(aq)}$ before and after contacting with the extraction phase, assuming no significant changes in liquid volumes and equilibrium mass transfer.

$$\text{Extraction efficiency} = \left[100 - \frac{\left([Ga]_{(aq,final)} \times 100\right)}{[Ga]_{(aq,init)}}\right] \quad (2)$$

$[Ga]_{(aq,init)}$ and $[Ga]_{(aq,final)}$ correspond to the initial and final gallium concentration in the aqueous phase, respectively.

Results and discussion

In the preliminary screening to determine which mixtures with TOPO formed room-temperature liquids, a range of hydrogen

bond donors (HBDs) were examined. All the materials tested are inexpensive, off-the-shelf chemicals (with the exception of 8-hydroxyquinoline-2-carboxylic acid), with relevance to separations in which TOPO has been used as an extractant. Table 1 lists all HBD–TOPO mixtures, their compositions expressed as a molar ratio of TOPO (χ_{TOPO}), and their apparent physical state, at room temperature and in a chilled state. For the purpose of the screening tests, the materials were used as received, without drying.

Long chain unsaturated fatty acids (palmitic and stearic) gave waxy solids, induced by the long alkyl chains of both components. Cellobiose (a disaccharide) produced a solid mixture rather than low melting liquids. Several phenolics that were screened – pyrogallol, resorcinol and gallic acid – all initially formed colourless liquids consistent with the previous results obtained with phenol. However, they all turned pink and subsequently brown over several days, which is likely to be due to oxidation to σ-benzoquinone (red) and subsequent reactions between σ-benzoquinone and remaining polyphenol to form coloured polymers comparable to the browning effect in fruit.[65–68] Nevertheless, a number of aromatic carboxylic acids, hydroxoacids and phenols gave colourless or yellow liquids at room temperature (Table 1).

The mixtures that formed room-temperature liquids at the tested molar ratio all have interesting potential applications. The combination of TOPO (a capping agent in nanoparticle synthesis) and catechol (a reducing agent) could be used as a medium for the synthesis of nanoparticles. This mixture appeared visually stable during prolonged storage, in contrast to similar mixtures with resorcinol, pyrogallol and gallic acid. However, freshly-made mixtures with the latter HBDs also could be investigated, taking advantage of TOPO (a weak base) enhancing their reducing ability.

The formation of liquid mixtures with phenolics, such as salicylic acid, gentisic acid, or 2,6-xylenol, suggests that neat TOPO could be used as a wide-range phenol extractant, forming TOPO–phenolic eutectics that would phase-separate from the aqueous phase (for example wastewater streams). The same strategy could be explored for the separation of levulinic and lipoic acids from fermentation broths.

Acetylacetone (acac)[69] and other β-diketones[70] have been shown to extract gallium from aqueous basic sources,[71] whereas TOPO diluted in hydrocarbon diluents (*e.g.* benzene) has been shown to extract gallium from acidic chloride sources.[31,72,73] The mixtures of TOPO with several HBDs: malonic acid, 8-hydroxyquinoline-2-carboxylic acid and diphenylacetic acid, all formed room-temperature liquids when combined with TOPO, highlighting their potential to form a TOPO-rich gallium extracting agent. Whereas the high cost of 8-hydroxyquinoline-2-carboxylic acid makes it unsuitable for industrial use, the combination of the low cost and β-carbonyl functionality in malonic acid makes it an industrially viable metal chelating agent.

Having identified a number of promising candidates, two unsaturated dicarboxylic acid systems were selected for further study, based on malonic and levulinic acids (Fig. 1).

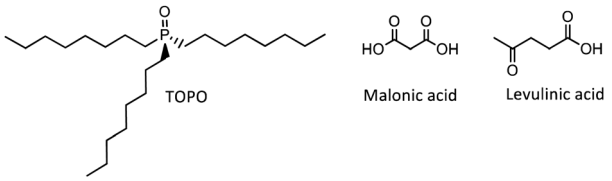

Fig. 1 Structures of TOPO, malonic acid and levulinic acid.

Both malonic acid and TOPO can act as ligands (complexing agents) for gallium. However, they have preferences for different gallium species, and therefore work best in different pH ranges, and it was hoped that their combination would result in a very robust extraction system. With regards to levulinic acid, it is the main product of the liquefaction of lignocellulosics occurring through acidic solvolysis or hydrolysis,[74] and is now recognised as one of the most important platform chemicals.[74–76] TOPO (30%) in methylisobutylketone (MIBK) has been used to extract levulinic acid from aqueous sulphuric acid feedstocks,[34] and this study could pave the way to a simplified approach with no auxiliary chemicals required.

Before in-depth studies were commenced, a rudimentary test for water miscibility was carried out across the range of liquid TOPO:malonic acid and TOPO:levulinic acid systems. In all cases they readily phase-separated, forming liquid–liquid biphases with water and aqueous hydrochloric acid (Fig. 2).

Thermal stability

The thermal decomposition of the TOPO:acid mixtures, as well as the pure components, was studied using dynamic TGA (10 °C min^{-1}), followed by isothermal studies.

TOPO:malonic acid. Dynamic TGA scans for the TOPO:malonic acid system (χ_{TOPO} = 0.00–1.00) are plotted in Fig. 3 with the thermal decomposition onset temperatures (T_d) and second stage of thermal decomposition onset (T_2) listed in Table 2. For ease of analysis, the changes in T_d and T_2 are plotted as a function of composition (χ_{TOPO}) in Fig. 4. Whereas both TOPO and malonic acid decomposed in a one-step process, the thermal decomposition of their mixtures occurred

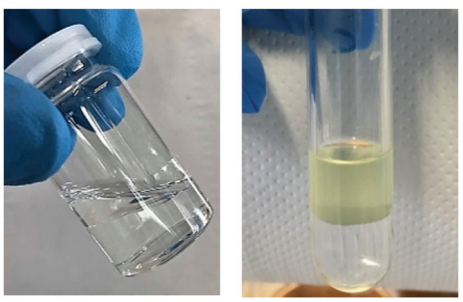

Fig. 2 Left: TOPO:malonic acid (χ_{TOPO} = 0.67) and water, forming a biphasic system with the TOPO:malonic acid eutectic as the less dense upper phase and water as the more dense lower phase. Right: TOPO:malonic acid (χ_{TOPO} = 0.67) and 6 M HCl forming a biphase with the TOPO:malonic acid eutectic as the less dense upper phase and aqueous HCl as the more dense lower phase. A yellow colour was added to help with visual distinction of the phases.

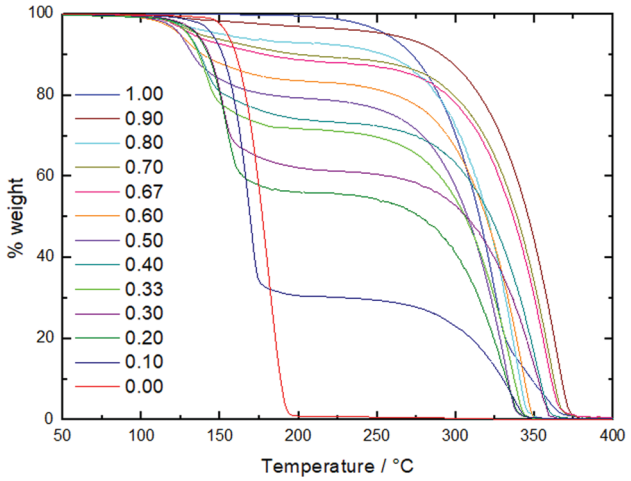

Fig. 3 Mass loss profile of TOPO:malonic acid mixtures under the TGA dynamic heating regime (10 °C min^{-1}) indicating two stage mixture decomposition.

Table 2 Onset of thermal decomposition (T_d) and second thermal decomposition step (T_2) for TOPO:malonic acid mixtures across the whole compositional range

χ_{TOPO}	T_d (onset)/°C	T_2/°C
1.00	204	—
0.90	103	235
0.80	99	227
0.70	92	236
0.67	90	239
0.60	89	233
0.50	86	231
0.40	83	237
0.33	82	232
0.30	99	236
0.20	100	232
0.10	113	239
0.00	133	—

with two distinct steps. In all mixtures, the first decomposition step was typically complete by *ca.* 200 °C, followed by the second step with a >225 °C onset (see the TGA and DTG example in Fig. S18, ESI†). The thermal decomposition was complete around 340–375 °C (Fig. 3).

The decomposition temperatures of neat TOPO and neat malonic acid, determined from the onset of mass loss, were determined to be T_d = 203 and 133 °C, respectively (red squares in Fig. 4). Kotova *et al.* found that the onset of TOPO thermal decomposition occurs at 149.9 °C using a Q-1500 derivatograph within a nitrogen atmosphere and using a scan rate of 10 °C min^{-1}.[77] This, however, does not align with our findings, which suggest that TOPO is thermally stable at temperatures up to 204 °C. The onset of mass loss from malonic acid corresponds to the literature values from Stanford *et al.* of 120–140 °C.[78] All mixtures decomposed in a two-step process, and T_d values were determined from the onset of mass loss in the first decomposition step (black squares in Fig. 4). The mixtures decomposed at slightly lower temperatures than neat malonic acid, in the range T_d = 82–113 °C. For acid-rich samples, the

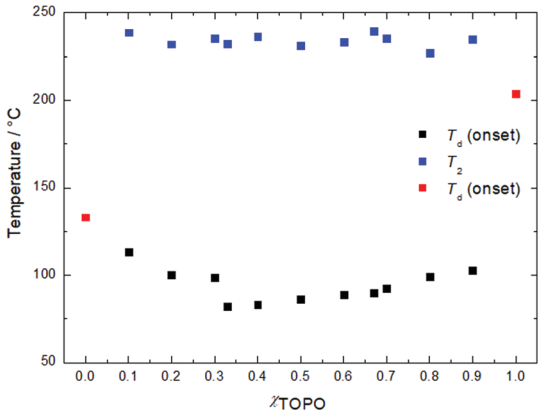

Fig. 4 Onset of mass loss in thermal decomposition stages one (black squares) and two (blue squares) in TOPO:malonic acid mixtures and neat components (red squares). Described as the thermal decomposition (T_d onset) and onset of mass loss in the second step (T_2) as a function of the TOPO mole ratio under TGA dynamic heating at 10 °C min^{-1}.

thermal stability decreased with increasing χ_{TOPO}, reaching a minimum at χ_{TOPO} = 0.33 (82 °C), where there is a molar ratio of two malonic acids per TOPO molecule. With a further increase in the TOPO mole fraction, the T_d values increased slightly.

To gain insight into the mechanism, the thermal decomposition of the χ_{TOPO} = 0.33 mixture was studied in detail. From isothermal TGA (22 h, 90 °C, Fig. 5), measured at a temperature close to the beginning of the first mass loss event, approximately 37% mass is lost after *ca.* 300 min, corresponding to loss of the malonic acid fraction in the first step (35% of the sample mass). The remaining 63% of the sample roughly corresponds to the TOPO content and decomposes in the second step (65% of the sample mass, see Fig. S16, ESI†). This is consistent with the pattern observed from the initial dynamic TGA (Fig. 3), where an approximate 29% mass loss is seen in the first step (some overlap between the decomposition of TOPO and malonic acid is justifiable under dynamic conditions). The initial

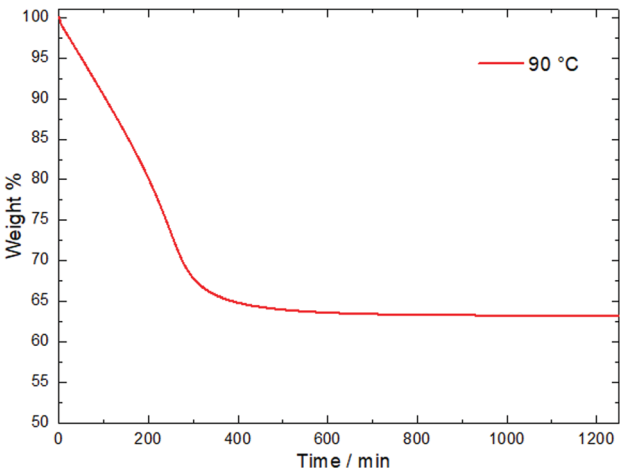

Fig. 5 Isothermal mass loss profile of χ_{TOPO} = 0.33 TOPO:malonic acid at 90 °C. Initial heating rate 50 °C min^{-1}.

decomposition rate in the first 3 h of the isothermal experiment (Fig. 5) was calculated to be 5.8% h^{-1}.

To investigate the chemical composition of both the gas and liquid, the same experiment was carried out on a larger scale (3 cm^3 of the χ_{TOPO} = 0.33 mixture was stirred at 90 °C, under a flow of argon). The composition of the gas phase was monitored using *in situ* GC-MS, and the composition of the liquid phase was probed after 1 h with ^1H and ^{13}C NMR spectroscopy. As the sample was held at 90 °C, bubbles were observed to form, the mixture turned cloudy, and there was a small amount of white crystalline material accumulated around the top of the round-bottomed flask. ^{13}C NMR spectroscopy confirmed the white powder to be malonic acid (Fig. S24, ESI†).

When sampling, there was a notable, pungent smell of vinegar from the decomposing sample, and the ^{13}C NMR spectrum (Fig. S22, ESI†) revealed the presence of acetic acid in the mixture after 1 h. Qualitative GC-MS detected large amounts of CO_2, as well as traces of CO and H_2O, in the gas phase (Fig. S19, ESI†). These results are aligned with decomposition of malonic acid *via* decarboxylation, producing acetic acid and carbon dioxide (eqn (3)).[78–83] This decomposition pathway has recently been reported also in choline chloride: malonic acid eutectics.[84]

$$CH_3(COOH)_2 \rightarrow CH_3COOH + CO_2 \quad (3)$$

Furthermore, trace amounts of detected CO and H_2O result most likely from the secondary decomposition of acetic acid (eqn (4) and (5)).[85]

$$CH_3COOH \rightarrow CH_4 + CO \quad (4)$$

$$CH_3COOH \rightarrow CH_2CO + H_2O \quad (5)$$

This pattern of mass loss *via* thermal decomposition (decarboxylation), combined with sublimation and evaporation (evidenced by malonic acid crystallising at the top of the flask), is common in many organic acids.[82] Compositions with low TOPO loading, up to χ_{TOPO} = 0.33, are not homogenous at the temperature of their decomposition (see the phase diagram, Fig. 11). It can be envisaged that malonic acid that is phase-separated from the mixture is free to sublime; with increased TOPO content, all malonic acid is hydrogen-bonded to TOPO and base-catalysed decarboxylation is dominant.

TOPO:levulinic acid. Dynamic TGA scans for the TOPO:levulinic acid system (χ_{TOPO} = 0.00–1.00) are plotted in Fig. 6, with the corresponding onset temperatures for mass loss (T_d) and the second (T_2) stage of thermal decomposition listed in Table 3 and plotted in Fig. 7. Most mixtures decomposed in a two-step process, in analogy to TOPO:malonic acid, with the exception of two compositions (χ_{TOPO} = 0.33 and 0.40), which decomposed in three steps (Fig. 7), featuring an additional, intermediate decomposition step (T_3). Examples of TGA and DTG plots corresponding to the three-step decomposition (Fig. 8, top and Fig. S28, ESI†) and two-step decomposition (Fig. 8, bottom and Fig. S27, ESI†) are deposited in this paper and in the ESI.† Furthermore, whereas the decomposition steps of the TOPO:malonic acid mixtures were clearly defined, for the TOPO:levulinic acid

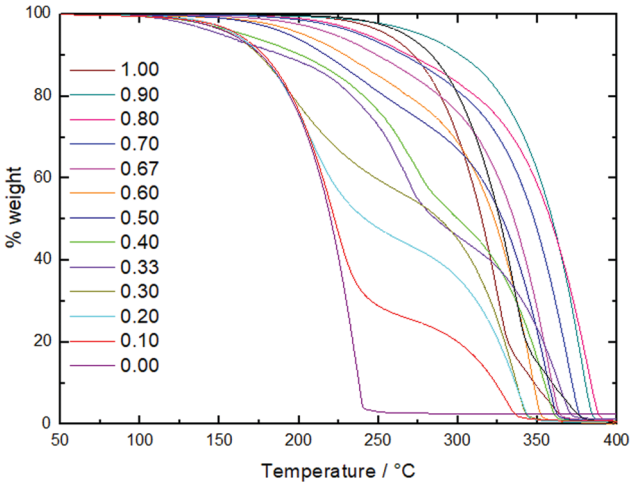

Fig. 6 Mass loss profile of TOPO:levulinic acid mixtures under the TGA dynamic heating regime (10 °C min^{-1}).

Table 3 Onset of thermal decomposition (T_d) for TOPO:levulinic acid mixtures across the whole compositional range

χ_{TOPO}	T_d (onset)/°C	T_2/°C	T_3/°C
1.00	204	—	—
0.90	198	303	—
0.80	181	273	—
0.70	169	279	—
0.67	155	273	—
0.60	141	276	—
0.50	130	276	—
0.40	108	304	198
0.33	92	308	179
0.30	102	272	—
0.20	106	276	—
0.10	106	273	—
0.00	107	—	—

mixtures there was much overlap between the steps (Fig. 8 and Fig. S18, S27 and S28, ESI†). Even reducing the heating rate to 1 °C min^{-1} (Fig. S29, ESI†) lead to no appreciable improvement in the resolution of the thermograms recorded for the TOPO:malonic acid mixtures.

The onset of mass loss, corresponding to decomposition of neat levulinic acid, was recorded at T_d = 106 °C (to the authors' surprise, no literature comparison was available). In mixtures with low TOPO content (up to χ_{TOPO} = 0.30), the T_d values remained similar to that of the neat acid. The χ_{TOPO} = 0.33 composition exhibited the lowest thermal stability (91 °C), in analogy with the behaviour observed in the TOPO:malonic acid system (Tables 2 and 3). However, a further increase in χ_{TOPO} resulted in a steady growth of the T_d values, several decades above the T_d value of neat levulinic acid (Fig. 7).

For neat levulinic acid and for mixtures with low TOPO loadings (χ_{TOPO} = 0.00 to 0.30) the onset of decomposition was consistently slightly above 100 °C, pointing to dehydration of levulinic acid. Loss of H_2O is consistent with formation of furanones (3,4-dihydro-6-methyl-2*H*-pyran-2-one) by water elimination from the enol form of the levulinic acid keto–enol equilibrium (eqn (6)).[86] The presence of TOPO is associated

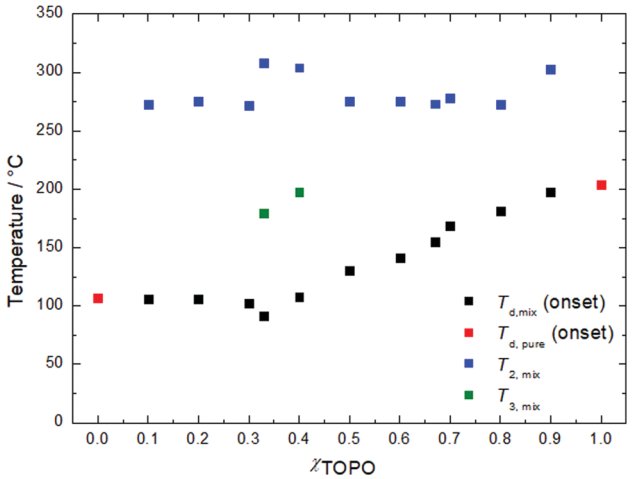

Fig. 7 Onset of mass loss in thermal decomposition stages one (black squares) and two (blue squares) and three (green squares) in TOPO:levulinic acid mixtures and neat components (red squares). Described as the thermal decomposition (T_d onset) and onset of mass loss in the second (T_2) and third (T_3) step as a function of the TOPO mole ratio under TGA dynamic heating at 10 °C min^{-1}.

with the second stage of decomposition (see Fig. 7 and an example of a DSC/DTG plot in Fig. 8, bottom).

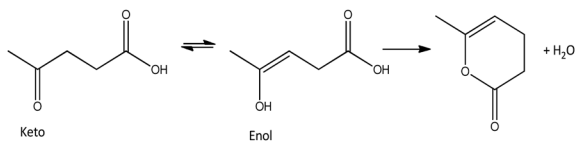

A marked change in the thermal decomposition pattern appears at χ_{TOPO} = 0.33, for which there is one mole of TOPO per two moles of carboxylic acid functionality present (and TOPO has been reported to preferentially interact with two hydrogen bond donors).[87] The TGA/DTG plots for χ_{TOPO} = 0.33 and 0.40 are very complex, with three groups of thermal events (Fig. 8, top, and Fig. S28, ESI†). The onsets of these events are plotted in Fig. 7. For both compositions, the first step appears to be related to water loss, and the last to thermal decomposition of TOPO, with a slightly higher onset of T_2 resulting from overlap with T_3. The middle event (T_3) is represented by a composite peak in the DTG curve, with two clearly-visible maxima and a shoulder. It is difficult to speculate what each of these features represents, but it can be assumed that they are related to loss/decomposition of levulinic acid from the sample.

Finally, compositions with high TOPO content (χ_{TOPO} = 0.50 to 0.90) are again characterised by a two-step decomposition (Fig. 8, bottom). The water loss feature is absent, and the first thermal event (T_d) appears to be in the same temperature range as the shoulder in the middle event of the DTG plot for χ_{TOPO} = 0.33 (Fig. 8, top). These mixtures are more stable than neat levulinic acid (Fig. 7), which can be rationalised by strong hydrogen-bonding with TOPO suppressing decomposition *via* water elimination. The first step of thermal decomposition was understood to arise from sublimation and evaporation/

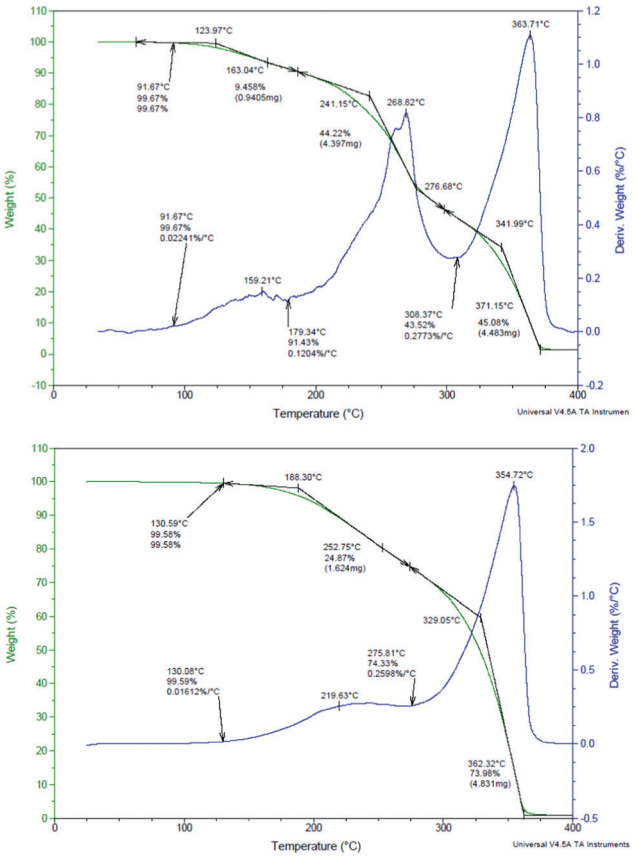

Fig. 8 TGA traces for TOPO:levulinic acid mixtures under dynamic heating at 10 °C min^{-1} from room temperature to 400 °C. The onset of each thermal event is depicted by arrows on the DTG plot (blue line). Top: χ_{TOPO} = 0.33 showing 3-stage mass loss – T_1 = 92 °C, T_2 = 308 °C, T_3 = 179 °C. Bottom: χ_{TOPO} = 0.50 showing 2-stage mass loss – T_1 = 130 °C, T_2 = 276 °C.

decomposition of levulinic acid, followed by thermal decomposition of TOPO.

Again, further study was focussed on the least stable composition, χ_{TOPO} = 0.33, which also displayed the most complex behaviour. Isothermal TGA study of the χ_{TOPO} = 0.33 sample at 90 °C (Fig. 9) revealed a lower rate of mass loss than for the analogous composition of TOPO:malonic acid (see the comparison in Fig. S34, ESI†).

At 90 °C, about 20% of the sample was lost after 500 min. The 20% loss accounts for more than dehydration (6% of the sample) but does not reach the mass loss of levulinic acid (38%), even after 2 days (2800 min). The mass loss rate was not constant, but decreased steadily, from the initial 4.0% h^{-1} to 2.6% h^{-1} after 2 h, and further decreased afterwards. This was contrasting with a steady loss of 5.8% h^{-1} over the first 3 h for the corresponding TOPO:malonic acid mixture, leading to the loss of the entire acid component. However, in the case of TOPO:levulinic acid, the continuous decrease in wt% (Fig. 9) suggests that a major route of mass loss is levulinic acid evaporation towards a liquid composition with a very low vapour pressure. The same experiment was repeated at 140 °C (Fig. 9 and Fig. S31–S33, ESI†), which led to a mass loss of

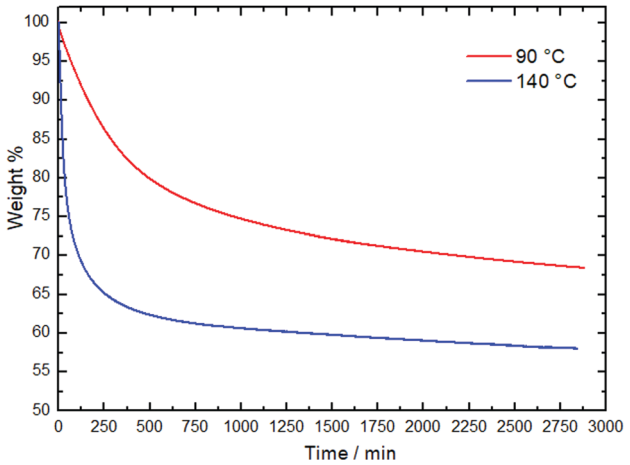

Fig. 9 Isothermal mass loss profile of separate χ_{TOPO} = 0.33 TOPO:levulinic acid mixtures at 90 °C and 140 °C. Initial heating rate 50 °C min^{-1}.

ca. 38% after 500 min, corresponding to removal of the levulinic acid component from the sample, and a much lower mass loss rate afterwards.

Based on the isothermal TGA studies, large-scale experiments were carried out at 125 and 140 °C, in order to reach an appreciable rate of thermal decomposition. In each case, a sample was heated in a round-bottomed flask (1 h, under a flow of argon), which resulted in the sublimation/evaporation of large quantities of a white solid that deposited as crystals around the neck of the flask (Fig. 10). This was identified as levulinic acid by ^{13}C NMR spectroscopy (Fig. S45, ESI†). Meanwhile, the liquid changed its appearance from colourless to yellow. The evolved gas analysis by *in situ* GC-MS indicated the loss of H_2O and CO_2, with the loss of H_2O increased significantly with increasing temperature from 125 to 140 °C (Fig. S34 and S35, ESI†).

The complicated appearance of the TGA/DTG thermogram (Fig. 8, top) can be justified by three processes occurring in parallel: sublimation/evaporation of levulinic acid, dehydration (eqn (6)) and decarboxylation to butanone (eqn (7)).[88,89]

$$CH_3C(O)(CH_2)_2COOH \rightarrow CH_3C(O)CH_2CH_3 + CO_2 \quad (7)$$

Fig. 10 Sublimation/evaporation of levulinic acid from the χ_{TOPO} = 0.33 TOPO:levulinic acid mixture, heated at 140 °C, under an argon flow, 60 min.

^{1}H NMR spectra of the post-thermolysis liquid (Fig. S41 and S43, ESI†) showed a reduction in the relative ratio of levulinic acid to TOPO when compared to the starting composition, but no decomposition products were identified. This can be justified by the tendency for further rapid decomposition of 3,4-dihydro-6-methyl-2*H*-pyran-2-one, and immediate evaporation of butanone (boiling point of 80 °C).[88]

Comparison of the thermal stability in both systems. Concluding the thermal stability study, it is demonstrated that the thermal stability of eutectics or similar mixtures must be carefully studied on a case-by-case basis, and no all-encompassing conclusions should be drawn. Whereas the TOPO:malonic acid mixtures had lower thermal stability than the neat acid, likely owing to a self-catalysing effect, the TOPO:levulinic acid liquids (χ_{TOPO} = 0.50 to 0.90) were significantly more stable than neat levulinic acid, preventing decomposition by dehydration. Similarly, with increasing TOPO content and the resulting likely elevation of the mixture boiling point, this would lead to a lower vapour pressure and smaller mass loss due to evaporation. Comparisons of the thermal decomposition onset of TOPO:malonic acid and TOPO:levulinic acid mixtures are presented in the ESI† (Fig. S47, ESI†).

Phase behaviour

Phase diagrams for the TOPO:malonic acid and TOPO:levulinic acid mixtures were constructed using the combination of differential scanning calorimetry (DSC) (Fig. S47–S70, ESI†) and visual observation of samples in a solid–liquid cell (SLC). Temperature (T_f) and enthalpy of fusion (ΔH_f) data for the pure components are summarised in Table S15 (ESI†).

Ideal liquidus phase boundaries were approximated (assuming activity coefficients γ_i = 1) using eqn (8), where χ_i is the mole ratio of component *i*, γ_i is the activity coefficient of component *i* at a given mole ratio, ΔH_f is the enthalpy of fusion of the neat components, R is the universal gas constant (8.314 J mol^{-1} K^{-1}), T_f is the temperature of fusion of the neat components (in K) and T is the temperature (in K). The specific heat capacity term was assumed to have an insignificant impact on the ideal liquidus phase boundary calculations ($\Delta_f C_p$ = 0), which is true for mixtures in which the neat components have similar melting points.[1,90,91]

$$\ln(\chi_i\gamma_i) = \frac{\Delta H_f}{R}\left(\frac{1}{T_f} - \frac{1}{T}\right) \quad (8)$$

TOPO:malonic acid. The TOPO:malonic acid mixtures formed homogeneous room temperature liquids between χ_{TOPO} = 0.55 and 0.67. Mixtures with lower TOPO loading (χ_{TOPO} = 0.10–0.50) were heterogenous at room temperature, containing both solid and liquid components, the proportion of the liquid component increasing with increasing χ_{TOPO} (χ_{TOPO} = 0.10 appeared solid). Furthermore, the χ_{TOPO} = 0.70 composition was biphasic (solid with a small quantity of liquid) and gradually solidified over the course of 2 weeks. All $\chi_{TOPO} > 0.70$ samples appeared solid at room temperature.

The phase diagram for TOPO:malonic acid was constructed using both DSC and SLC results and is shown in Fig. 11. DSC scans

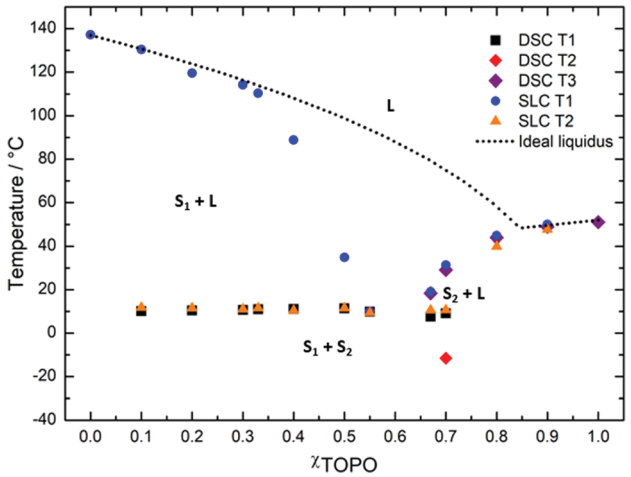

Fig. 11 Phase diagram for TOPO:malonic acid mixtures across the whole compositional range. Constructed from SLC and DSC results. S = solid, L = liquid.

were recorded over the range −90 to 70 °C and maxima of all first-order endothermic phase transitions (melting events) were recorded. However, some thermal events were close to (or above) the onset of thermal decomposition temperature (T_d) of the corresponding samples, and therefore not accessible through DSC. SCL experiments could be carried out above T_d, without concern about damage to the apparatus; however, it should be noted that the χ_{TOPO} = 0.00–0.33 samples turned yellow upon melting. The respective observed transition temperatures are shown in Table 4.

The phase diagram for TOPO:malonic acid shows characteristic simple eutectic behaviour of the mixtures classified by Nývlt as one in which the components do not form a compound and are miscible and immiscible in the liquid and solid phases, respectively.[92] In the region $\chi_{TOPO} < 0.60$, the phase behaviour is uncomplicated. Endothermic peaks associated with the melting point of the eutectic composition (*ca.* 11 °C) are evident from DSC (DSC T_1) and are in very good agreement with the onset of stirring bar movement in SLC (SLC T_2). Furthermore,

Table 4 Data used to construct the TOPO:malonic acid phase diagram

	Phase change temperature/°C					
	DSC			SLC		
χ_{TOPO}	T_1	T_2	T_3	T_1	T_2	T_g
0.00	—	—	—	137	—	—
0.10	10	—	—	130	12	—
0.20	10	—	—	120	12	—
0.30	11	—	—	114	11	—
0.33	11	—	—	110	12	—
0.40	11	—	—	89	11	—
0.50	11	—	—	35	12	—
0.55	10	—	—	10	10	—
0.60	—	—	—	—	—	−4
0.67	8	—	18	19	11	—
0.70	9	−12	29	31	11	—
0.80	—	—	44	45	40	—
0.90	—	—	49	50	48	—
1.00	—	—	52	52	—	—

the liquidus point observed using the solid–liquid cell (SLC T_1) corresponds to melting of excess malonic acid.

On the TOPO-rich side of the phase diagram, $\chi_{TOPO} > 0.70$, data recorded as DSC T_3, SLC T_1 and SLC T_2 all trace the melting point of samples that are solid at room temperature, and all melt to give clear liquids at, or below, 50 °C. There was no evidence of eutectic melting at $\chi_{TOPO} > 0.70$. However, 'wet patches' were found in a χ_{TOPO} = 0.80 sample left at 30 °C overnight, suggesting that the dissolution of TOPO is very slow in samples at $\chi_{TOPO} > 0.70$.

Compositions χ_{TOPO} = 0.67 and 0.70 displayed more complex phase behaviour. For example, the DSC scan for χ_{TOPO} = 0.67 (Fig. S57, ESI†) features two first-order, endothermic phase transitions, accompanied by a broad, two-stage cold-crystallisation and an additional crystallisation upon cooling.

At χ_{TOPO} = 0.70 there is a low temperature transition noted as DSC T_2; however, it is likely that this is a solid–solid transition. Again, the onsets of stirring bar movement in SLC (SLC T_2) and DSC T_1 are aligned and correspond to the melting of the eutectic composition. The highest-temperature feature in the DSC measurements (DSC T_3) aligns with the observed liquidus points (SLC T_1) and corresponds to the melting of TOPO in the mixtures.

Finally, the χ_{TOPO} = 0.55 sample exhibited one first order transition in the DSC trace, which lies along the line corresponding to the observed eutectic isotherm line, and the χ_{TOPO} = 0.60 sample is the only composition that does not feature a first-order transition in a DSC scan. Rather, there was a glass softening observed in the SLC, reported as the onset of stirrer bar movement, SLC T_g (−4 °C), with inhibited crystallisation resulting from the mixture heterogeneity. This increases the extent of disruption and frustration of packing of species within a single crystalline lattice. TOPO:dodecanoic acid mixtures have been reported by the Kroon group, whereby the eutectic point lies at χ_{TOPO} = 0.43.[47]

It is expected that below the horizontal solidus line (*ca.* 11 °C) corresponding to the observed eutectic isotherm, the samples are heterogenous solids. Above the highest melting points plotted, an unsaturated, homogenous solution exists and between these lines saturated solutions co-exist with crystals of the neat components. There was no evidence of melting at *ca.* 11 °C in the samples above χ_{TOPO} = 0.70 using the DSC and SLC apparatus; however, it is likely that kinetic effects hamper the detection of the eutectic composition in these samples.

TOPO:levulinic acid. The phase diagram for TOPO:levulinic acid (Fig. 12 and Table 5) differs from that for TOPO:malonic acid, arguably because levulinic acid has only one carboxylic acid group and there is a large difference in the melting points of the pure malonic acid and levulinic acid components (137 and 32 °C, respectively). These mixtures exhibit characteristic eutectic profiles with the lowest temperature melting point in the region around χ_{TOPO} = 0.40. This is consistent with other TOPO mixtures with phenol[48] and dodecanoic acid.[47]

At room temperature, the samples within the χ_{TOPO} = 0.10–0.20 composition region were biphasic, containing mostly

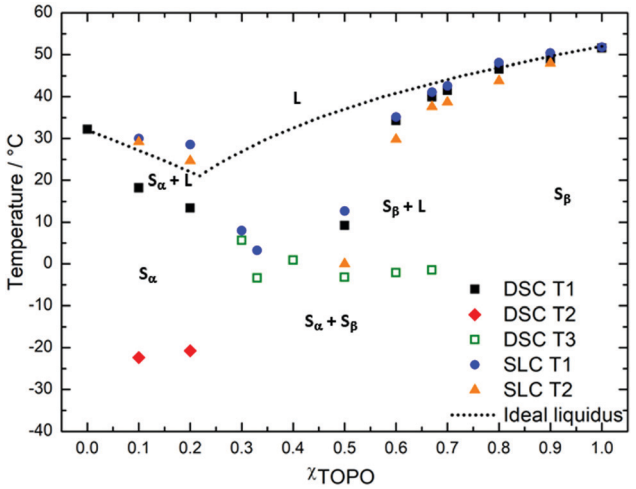

Fig. 12 Phase diagram for TOPO:levulinic acid mixtures across the whole compositional range. Constructed from SLC and DSC results. S = solid, L = liquid.

Table 5 Data used to construct the TOPO:levulinic acid phase diagram

	Phase change temperature/°C					
	DSC			SLC		
χ_{TOPO}	T_1	T_2	T_3	T_1	T_2	T_g
0.00	32	—	—	—	—	—
0.10	18	−22	—	30	29	—
0.20	13	−21	—	29	25	—
0.30	—	—	6	8	—	−14
0.33	—	—	−3	3	—	−24
0.40	—	—	1	—	—	−36
0.50	9	—	−3	13	0.0	—
0.60	34	—	−2	35	30	—
0.67	40	—	−2	41	38	—
0.70	42	—	—	43	39	—
0.80	47	—	—	48	44	—
0.90	49	—	—	50	48	—
1.00	52	—	—	52	—	—

liquid with a small quantity of suspended solid. The corresponding part of the phase diagram (Fig. 12) features the liquidus line slightly above ambient temperature (as recorded from the solid–liquid cell, SLC T_1 and SLC T_2), corresponding to melting of excess levulinic acid. From the DSC data, a phase transition at/slightly below ambient temperature (DSC T_1) corresponds to a melting event. In addition, DSC revealed a low-temperature endothermic event at *ca.* −20 °C (DSC T_2), possibly indicating the transition between heterogeneous conjugated solid phases of TOPO and levulinic acid and a levulinic acid solid solution with TOPO acting as the solute in a levulinic acid matrix 'S_α'.

Compositions χ_{TOPO} = 0.30–0.50 were homogenous liquids at ambient temperature. Finally, the DSC scans for the χ_{TOPO} = 0.30–0.40 compositions featured low-enthalpy first-order events (Fig. S64–S66 in the ESI†).

On the TOPO-rich side of the phase diagram, the χ_{TOPO} = 0.50 mixture forms a liquid at room temperature, whereas increasing χ_{TOPO} to 0.60 generated a gel with liquid entrapped within a solid matrix. At $\chi_{TOPO} > 0.67$, the mixtures formed solids under ambient conditions. In the phase diagram, for $\chi_{TOPO} > 0.50$, data recorded as DSC T_1, SLC T_1 and SLC T_2 trace the melting point of samples that melted in a single event to give clear liquids. The liquidus point was below ambient for the χ_{TOPO} = 0.50 mixture, which aligns well with the preliminary visual observation. Furthermore, low enthalpy first order events in χ_{TOPO} = 0.30–40, a broad shoulder in the χ_{TOPO} = 0.50–67 compositions (DSC T_3), and SLC T_2 for χ_{TOPO} = 0.50 trace a line corresponding to a eutectic isotherm that melts around *ca.* −2 °C.

It is thought that the TOPO:levulinic acid phase diagram is of type 2-IIIa, following the binary system classification by Nývlt.[92] The pure components have close melting points (χ_{TOPO} = 0.00 and 1.00 melt at 32 and 51 °C, respectively) and partial miscibility in the solid phase. Therefore, below the horizontal solidus line (*ca.* −2 °C) corresponding to the observed eutectic isotherm, the samples are heterogenous conjugated solids. The regions identified as 'S_α' and 'S_β' correspond to levulinic acid and TOPO solid solutions, respectively, whereby there is partial miscibility between the components as a solute of one component within a matrix of the other. Above the highest melting points plotted, an unsaturated, homogenous TOPO:levulinic acid solution exists and between the lines representing homogenous unsaturated solutions and solid solutions lie saturated solutions which co-exist heterogeneously with levulinic acid 'S_α' and TOPO 'S_β' solid solutions.

Discontinuous solid solutions of this type are common in binary phase diagrams of fatty mixtures[93] and result from structural differences between components.[94]

^{31}P NMR spectroscopy

TOPO:acid mixtures that were liquid at ambient temperature were studied neat using ^{31}P NMR spectroscopy to examine the strength of interactions of TOPO with the acids.

The ^{31}P chemical shift for free TOPO (χ_{TOPO} = 1.00) varies with both the solvent (for example, δ_{31P} = 45.37 ppm in d_6-acetone compared to *ca.* 46 ppm in d_3-acetonitrile[95]) and concentration. This environmental response can be used as a measure of the degree of interaction with acids: in the presence of coordinating strong Lewis acids, the chemical shift can reach values around δ_{31P} = 75–85 ppm for liquid coordination complexes of $AlCl_3$ and $GaCl_3$ (which gives up to a $\Delta\delta_{31P}$ = +36 ppm downfield shift).[44] The body of relevant literature is even richer for triethylphosphine oxide (TEPO), which is used as the ^{31}P NMR probe of Lewis acidity[96,97] and hydrogen bond strength.[98]

In this context, the liquid TOPO:malonic acid (Fig. S73, ESI†) and TOPO:levulinic acid (Fig. S74, ESI†) mixtures exhibit ^{31}P chemical shifts over the range δ_{31P} = 53–57 ppm ($\Delta\delta_{31P}$ = +8–12 ppm), demonstrating strong hydrogen bonding. These results are very similar to work previously conducted by the group studying a TOPO:phenol system;[48] as in our earlier work, there is a $\Delta\delta_{31P}$ = 1.6–2.0 ppm downfield shift for each subsequent χ_{TOPO} = 0.1 increment, following a linear trend (Fig. 13).

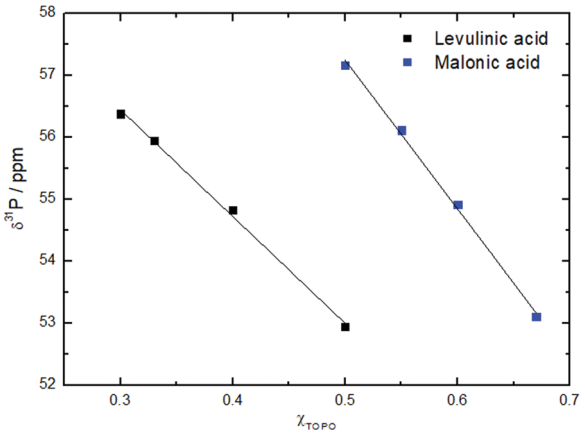

Fig. 13 ^{31}P NMR chemical shifts as a function of χ_{TOPO} in TOPO:malonic acid and TOPO:levulinic acid liquid samples.

When the magnitudes of the ^{31}P NMR chemical shifts recorded for different χ_{TOPO} values are compared in terms of hydrogen bonding motifs (Table 6), the shifts in signal experienced in the presence of one or two hydrogen-bonding carboxylic acid groups are remarkably similar and independent of the acids.

From this analysis, it can be inferred that the strength of interaction of carboxylic acids with TOPO depends chiefly on the ratio of carboxylic acid units to TOPO given that these acids all have largely similar pK_a values. In the solid state, equimolar mixtures of triphenylphosphine oxide with benzoic acids exhibit one hydrogen bond per phosphine oxide functionality.[99,100] However, it is also known that the phosphine oxide (P═O) moiety can exhibit an ''ambidextrous'' nature in hydrogen bonding in the solid state, whereby it can participate in more than one simultaneous hydrogen bond without compromising their strength in negative cooperativity.[87] Furthermore, studies focusing on the electron localisation function suggest that the phosphine oxide functionality has the potential to participate in up to three simultaneous hydrogen bonds in the solid state.[87,101,102] It is thought that this ambidextrous nature should also characterise the liquid state.[87]

If this is interpreted in the context of partitioning of the acid between the aqueous and TOPO-rich phase, this suggests that since all acids interact in a similar manner at the H-bonding site, a key difference to selective extraction and/or prevention of leaching is the hydrophobicity of the acid itself. This is in agreement with van den Bruinhorst *et al.*, who showed that the distribution coefficient of volatile fatty acids (VFAs) between a TOPO eutectic and an aqueous phase followed butyric > propionic > acetic acid, indicating that extraction of these VFAs is based on the extent of acid hydrophobicity.[47]

Table 6 ^{31}P chemical shifts associated with TOPO:malonic acid and TOPO:levulinic acid liquid samples. Neat, D_3PO_4 capillary, 25 °C

TOPO : acid unit	χ_{TOPO}	δ^{31}P/ppm	χ_{TOPO}	δ^{31}P/ppm
	TOPO:malonic acid		TOPO:levulinic acid	
			0.30	56.38
1 : 2	0.50	57.17	0.33	55.95
	0.55	56.12		
	0.60	54.92	0.40	54.84
1 : 1	0.67	53.11	0.50	52.95

Density

Differential densities between the two phases are important for the ease of separations. Densities of TOPO:malonic acid and TOPO:levulinic acid liquid mixtures were recorded within the temperature range of 20–50 °C, at 5 °C increments.

The densities and molar volumes of TOPO:malonic acid mixtures, plotted as a function of temperature (Fig. 14 and tabulated in Tables S16 and S17, ESI†), show a density decrease and molar volume increase with increasing χ_{TOPO}. This is expected, as TOPO is less dense than malonic acid (ρ_{TOPO} = 0.861 g cm^{-3}, ρ_{MA} = 1.62 g cm^{-3}). The density and molar volume of each liquid sample also decrease and increase linearly, respectively, with increasing temperature.

The densities of TOPO:levulinic acid mixtures, plotted as a function of temperature (Fig. 15 and tabulated in Tables S16 and S17, ESI†), reveal a similar pattern of a density decrease

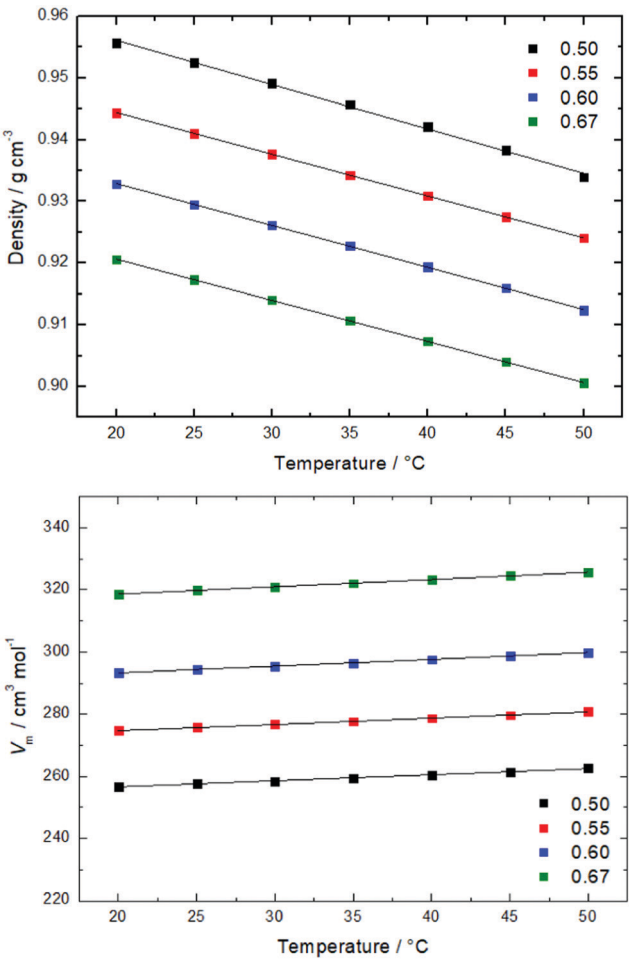

Fig. 14 Top: Density of TOPO:malonic acid liquid mixtures as a function of temperature. Bottom: Molar volume (V_m) of TOPO:malonic acid liquid mixtures as a function of temperature.

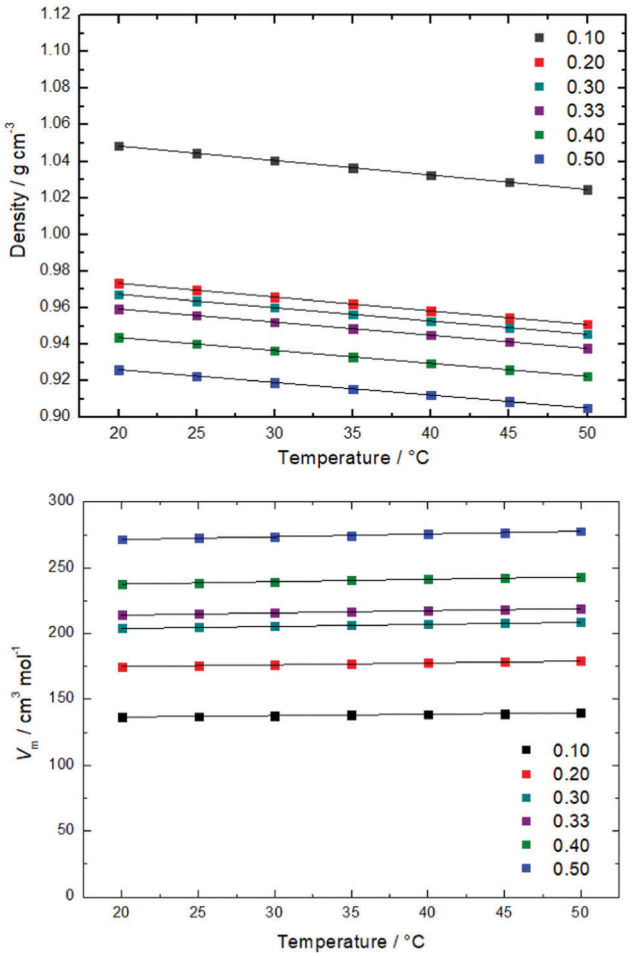

Fig. 15 Top: Density of TOPO:levulinic acid liquid mixtures as a function of temperature. Bottom: Molar volume (V_m) of TOPO:levulinic acid liquid mixtures as a function of temperature.

and molar volume increase with increasing χ_{TOPO} value and with increasing temperature. However, the χ_{TOPO} = 0.10 sample is significantly more dense than the other systems; this is speculated to be due to the liquid structure of this sample being very similar to that of levulinic acid ($\rho_{levulinic\ acid}$ = 1.12738 g cm^{-3}, 35 °C).[103] The molar volumes in this case show that this is a result of the large molar mass difference between TOPO (386.63 g mol^{-1}) and levulinic acid (116.12 g mol^{-1}) as expected.

The data were plotted as a function of temperature and fitted to linear equations $\rho = a + bT$ and $V_m = a + bT$ where a is the y axis intercept, b is the gradient of the line, ρ is density (g cm^{-3}), V_m is the molar volume (cm^3 mol^{-1}) and T is temperature (°C). The equation parameters and absolute average deviation of the fits are plotted in Table 7 and Table S18 (ESI†), respectively. Residual plots can be found in Fig. S75 and S78 (ESI†). A slightly better fit was achieved with a polynomial; however, we were hesitant to risk overinterpretation with this unusual fit to density/molar volume data, considering that the residuals are within the error of the measurement.

Calculation of excess molar volumes (V_m^E) would be beneficial to better understand the interactions occurring in these liquids.

Table 7 Fitting parameters from linear regression of the density and molar volume data for TOPO:malonic acid and TOPO:levulinic acid liquid mixtures as a function of temperature over the range 20–50 °C. The units for a and $-b$ for the density data are g cm^{-3} and g cm^{-3} °C^{-1}, respectively, and the units for a and b for the molar volume data are cm^3 mol^{-1} and cm^3 mol^{-1} °C^{-1}, respectively

		Density (ρ)		Molar volume (V_m)	
Mixture	χ_{TOPO}	a	$-b$	a	b
TOPO:malonic acid	0.50	0.9705	0.0007	252.6	0.1973
	0.55	0.9580	0.0007	270.7	0.2016
	0.60	0.9465	0.0007	288.9	0.2187
	0.67	0.9340	0.0007	313.9	0.2358
TOPO:levulinic acid	0.10	1.0644	0.0008	134.4	0.1061
	0.20	0.9883	0.0007	172.1	0.1378
	0.30	0.9819	0.0007	200.8	0.1569
	0.33	0.9738	0.0007	210.8	0.1645
	0.40	0.9578	0.0007	234.0	0.1823
	0.50	0.9399	0.0007	267.3	0.2076

However, as one or more neat components are solid in the temperature range studied, the inevitable volume expansion with liquification would obscure results, resulting in positive V_m^E values, which are not representative of the interactions occurring in the mixtures.

In conclusion, when extraction applications are concerned, compositions with lower acid loadings (high χ_{TOPO} values) lend themselves to be the best choice. They are characterised by the lowest density (potentially facilitating phase separation from the aqueous phase) and have a slightly stronger interaction between TOPO and the acid, which may help to limit leaching.

Leaching study

TOPO has very low solubility in water (0.15 mg L^{-1})[104,105] and has been shown not to contaminate the aqueous phase when considering the TOPO:phenol DES.[48] In this work, therefore, the studies on the aqueous stability of the χ_{TOPO} = 0.55 and 0.67 TOPO:malonic acid mixtures focus on malonic acid leaching. The two compositions selected were at the opposite extremities of the liquid range. A summary of the leaching study results is shown in Table 8.

Aligned with earlier observations for the TOPO:phenol system,[48] the hydrogen bond donor (*i.e.* malonic acid) was

Table 8 Malonic acid[a] leaching from the eutectic phase into the aqueous phase after contact. Equivolume org : aq, ambient temperature, shaking time: 20 min. At 25 °C: 107.8 g L^{-1} malonic acid in χ_{TOPO} = 0.67 TOPO:malonic acid and 150.2 g L^{-1} malonic acid in χ_{TOPO} = 0.55 TOPO:malonic acid

		$[Malonic\ acid]_{aq}$/g L^{-1}		Mass loss at single contact/%$_{Malonic\ acid}$		
[HCl]/M	χ_{TOPO}	FT-IR	TOC	FT-IR	TOC	Average
0	0.67	15	14	14	13	14
	0.55	59	56	39	37	38
6	0.67	—	50	—	46	—
	0.55	—	92	—	61	—

[a] Malonic acid solubility in H_2O = 763 g L^{-1} at 25 °C.[106]

found to measurably leach from the TOPO:malonic acid mixture into the aqueous phase. The TOPO-rich composition used in gallium extraction (χ_{TOPO} = 0.67) moderately leached malonic acid into deionised water (13–14% of the malonic acid mass was lost). Unfortuantely, this percentage rose significantly when the mixture was contacted with 6 M HCl (46% loss at the HCl acid concentration yielding the optimum gallium extraction efficiency). In contrast with TOPO:phenol systems, the leaching is highly sensitive to the pH of the aqueous phase. The χ_{TOPO} = 0.55 mixture showed even greater propensity to leach malonic acid than the χ_{TOPO} = 0.67 mixture, resulting from the relative increase in the initial malonic acid content: 150 *vs.* 108 g L^{-1}, respectively. The difference can be justified in terms of stronger interaction with TOPO in the latter case, as indicated by the ^{31}P NMR study (Fig. 13). This highlights the importance of designing extracting liquids with the highest mole ratio of TOPO possible, in order to limit the leaching of malonic acid.

As a result of this leaching, the composition of the organic TOPO:malonic acid eutectic mixture changed after contact with an aqueous phase (Table S19, ESI†). This compositional change is of particular interest when considering these TOPO:malonic acid eutectic mixtures as extractants. Taking the χ_{TOPO} = 0.67 mixture as an example and using a 6 M HCl aqueous phase due to its relevance in our test application, the TOPO mole ratio with respect to malonic acid is altered to χ_{TOPO} = 0.79 (*i.e.* $\Delta\chi_{TOPO}$ = 0.12). However, circling back to the TOPO:malonic acid phase diagram (Fig. 11 and Table 4) shows that, in contrast to what we observed, a χ_{TOPO} = 0.79 TOPO:malonic acid mixture would exhibit solid phase behaviour at this composition at ambient temperature (*i.e.* this compositional change would cross the solid–liquid phase boundary). Therefore, as the TOPO:malonic acid mixture remained in a liquid phase after pre-contact with 6 M HCl, this suggests that partial transfer of de-ionised water or aqueous HCl in the pre-contacting stage must occur in order to keep the organic phase liquified.

Despite leaching, malonic acid in aqueous streams does not raise the same level of concern as phenolic contaminated waste-water, as an environmentally benign and readily biodegradable compound.[107] For an industrially-viable application, however, a longer-chain, more lipophilic analogue could be explored.

Test application: liquid–liquid gallium extraction from aqueous acidic chloride feedstock using TOPO:malonic acid

In order to demonstrate the potential for application of TOPO-based eutectics, the TOPO:malonic acid system was screened in a model extraction of gallium(III) from an aqueous feed. In general, gallium is extracted as a secondary element from acidic or basic waste streams, the former originating from zinc leach residue and LED waste and the latter from aluminium manufacturing waste (*e.g.* Bayer solutions or red mud).[71,73,108] TOPO has been known to extract gallium from acidic chloride sources with dilution in a hydrocarbon diluent, the limiting factor being the solubility limit of TOPO.[31,72,73] The concentrated TOPO-rich liquids reported here appear to be the perfect solution to this problem. Furthermore, acetylacetone (acac)[69] or various β-diketone[70] functionalities have been reported to extract gallium from strongly basic aqueous sources, although their chemical instability under basic conditions has prevented commercial use.[71] In the acidic regime, however, carboxylic acids have been reported to extract gallium from dilute acidic chloride solutions.[73,109,110] This, and the knowledge of gallium chloride forming liquid hydrophobic adducts with TOPO,[44] has led to the test use of a TOPO:malonic acid eutectic in an acidic chloride aqueous feed, in the hope to reap a synergistic benefit of both components potentially involved in extraction.

As indicated earlier in this paper, the χ_{TOPO} = 0.67 composition appears to be the best choice of extractant, being an ambient-temperature liquid with a high TOPO concentration, low density and strong affinity to the acid (for leakage prevention).

Extraction of gallium from acidic chloride aqueous phases was tested across a range of HCl concentrations, and compared to a standard benchmark (0.004 M TOPO in benzene, 6 M HCl containing 0.00568 M $GaCl_3$), replicating conditions reported previously by Sato *et al.*[31] A comparison of the results from this work and the benchmark is shown in Fig. 16 (and tabulated in Table S20, ESI†).

The extraction efficiency increases with increasing HCl concentration. This is due to the increased tendency to form $[GaCl_4]^-$ in the aqueous phase at higher HCl concentrations,[111] whereas $GaCl_3$ and/or the products of hydrolysis (*e.g.* $Ga(OH)Cl_2$ or $Ga(OH)_2Cl$) are the dominant species at lower HCl concentrations resulting from the strong propensity for $GaCl_3$ to hydrolyse at low acid concentrations, the degree of which can be calculated.[112–114] Tetrachlorogallate(III) anions, $[GaCl_4]^-$, are reported to be extracted *via* solvent extraction with a proton with TOPO at high acid concentrations. However, in order to unveil the underlying extraction mechanism in the case of χ_{TOPO} = 0.67 TOPO:malonic acid both the content of water in the organic phase and whether or not HCl is exchanged with

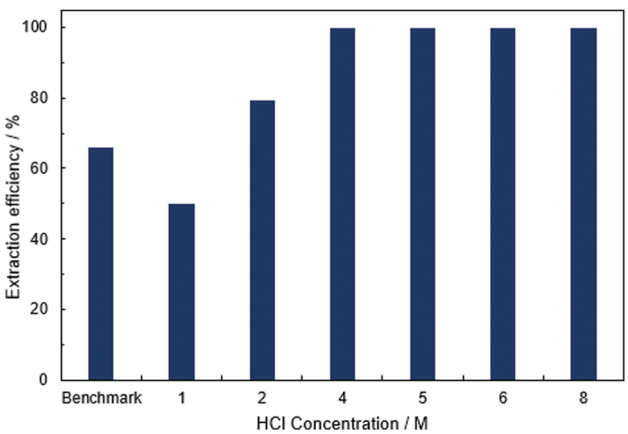

Fig. 16 Extraction of gallium from an aqueous acidic chloride feed across a range of HCl concentrations from 1–8 M using χ_{TOPO} = 0.67 TOPO:malonic acid, compared to a benchmark extractant of 0.004 M TOPO in benzene. Conditions: ambient temperature, initial $GaCl_3$ concentration = 0.00568 M, org : aq 1 : 1, pre-contact time 10 min, extraction time 10 min.

Table 9 Amount of gallium extracted (mmol) from the aqueous phase by χ_{TOPO} = 0.67 TOPO:malonic acid when TOPO is in excess of gallium ([$GaCl_3$] = 0.006 M) and when gallium is in excess of TOPO ([$GaCl_3$] = 0.504 M). Ambient temperature, pre-contact time: 10 min, extraction time: 10 min. When $[GaCl_3]_{aq}$ = 0.006 M, org : aq = 1 : 1. When $[GaCl_3]_{aq}$ = 0.504 M, org : aq = 1 : 5. The D_{Ga} values are gallium distribution coefficient estimates

Initial $[GaCl_3]_{aq}$/M	[HCl]/M	Ga extracted/M	D_{Ga}
0.00568	1	0.00294	0.98
	5	0.00502	3499
	6	0.00562	3914
	8	0.00516	3599
0.504	1	0.792	0.51
	5	1.18	1.35
	6	1.34	1.53
	8	1.28	1.37

the carboxylic acid of the extractant following pre-equilibration should be followed in the future.

Under the conditions optimised by Sato *et al.* (6 M HCl, 20 °C),[31] the TOPO concentration is limited by its solubility in benzene, and the single contact distribution ratio was *ca.* D_{Ga} = 1.3 (as read from a log graph reported). However, upon reproducing this experiment, the maximum benchmark single-contact gallium extraction efficiency was 66% (D_{Ga} = 1.96). It is noteworthy that the literature value was calculated from eqn (8) ([Ga_{org}] is the concentration of gallium in the organic phase, [Ga_{aq}] is the concentration of gallium in the aqueous phase), for which [Ga_{org}] was quantified by stripping the organic phase with an acidified aqueous phase, and subsequent measurement of the gallium concentration in the aqueous phase. This assumes that no gallium remained in the organic phase.

$$D_{Ga} = \frac{[Ga_{org}]}{[Ga_{aq}]} \quad (9)$$

D_{Ga} was calculated from eqn (9). This assumes equilibrium mass transfer and no significant change in liquid volume as the gallium content in the organic phase was not measured directly.

The value of D_{Ga} = 1.96 was used as a benchmark. Following reproduction of the benchmark experiment (TOPO in benzene), the χ_{TOPO} = 0.67 TOPO:malonic acid mixture was tested under identical conditions. As expected, all gallium was extracted from aqueous feeds at acid concentrations of 4 M HCl and above (to the detection limit of 0.1 ppm). These results primarily arise from a significantly greater concentration of TOPO in the eutectic extracting phase compared to the benchmark TOPO in benzene solution, which demonstrates the validity of this approach.

Given that complete extraction of gallium was achieved using the χ_{TOPO} = 0.67 TOPO:malonic acid liquid extractant and the large excess of TOPO present in the liquid, the loading capacity of the extractant was studied. The results of the χ_{TOPO} = 0.67 TOPO:malonic acid loading capacity are shown in Table 9 and represent the amount of gallium extracted (mmol) per mL of extractant when contacted with concentrated HCl solutions containing *ca.* 0.5 M gallium chloride.

When the literature benchmark was replicated using 0.004 M TOPO dissolved in benzene and contacted 6 M HCl containing 0.00568 M $GaCl_3$, 0.00372 mmol mL^{-1} gallium was extracted. The results show that the loading capacity of the χ_{TOPO} = 0.67 TOPO:malonic acid extractant is approximately 3 orders of magnitude greater than that achieved by the literature benchmark under the same conditions (*i.e.* 0.00372 and 1.34 mmol mL^{-1}, respectively). This suggests that the χ_{TOPO} = 0.67 TOPO:malonic acid extractant has the potential to be used in multiple stage contact during extraction due to its large loading capacity.

Conclusions

Mixtures of TOPO with HBDs were screened to identify those that yield room-temperature liquids, with the potential for applications in separations. A range of such mixtures were identified, and from these two systems were selected for in-depth study: TOPO:malonic acid and TOPO:levulinic acid, the former of interest for bifunctional gallium extraction, the latter potentially useful for the separation of levulinic acid from bio-derived mixed feeds.

Thermal analysis of the TOPO:malonic acid and TOPO:levulinic acid mixtures gives valuable insight into the operational condition limits. It was shown that, depending on the thermal decomposition pathway, the presence of TOPO can decrease or increase the thermal stability of the acid component. The phase diagrams were dependent on the acid structure: TOPO:malonic acid exhibited simple eutectic behaviour,[92] in which the components did not form a compound and were miscible and immiscible in the liquid and solid phases, respectively. Similarly, TOPO:levulinic acid had a solid liquid equilibrium where the components did not form a compound and were miscible in the liquid phase; however, in contrast to the TOPO:malonic acid phase diagram, the components were partly miscible in the solid phase, therefore exhibiting a 2-III_a type phase diagram.[92] The lowest-transition composition was χ_{TOPO} = 0.55 in TOPO:malonic acid; however, it must be noted that χ_{TOPO} = 0.60 acted as a glass and therefore did not exhibit melting, but instead exhibited glass softening in the heating cycle. TOPO:levulinic acid's lowest transition composition was χ_{TOPO} = 0.40.

When considering applications in extraction, a rational approach is to work with compositions that have a high percentage of TOPO and yet remain liquid at ambient temperature, rather than with eutectic compositions. Using ^{31}P NMR spectroscopy, it was shown that such TOPO-rich compositions have stronger interactions with HBDs, and therefore should limit leaching of the HBD component to the aqueous phase. This was confirmed with leaching studies which indicated that higher χ_{TOPO} values resulted in lower leaching levels to both a water phase and a 6 M HCl aqueous phase independently. Unfortunately, the leaching increased with increasing acidity of the aqueous phase. From density studies, TOPO-rich mixtures

have lower density, which could enhance phase separation from water. Finally, depending on the process, maximising the TOPO concentration might be beneficial for the extraction efficiency.

In conclusion, this work proposes a new route to bifunctional, liquid, solvent-free extracting agents, underpinned by useful physico-chemical insights to guide future formulations. It is expected for this physical chemistry study to inspire further investigation into TOPO mixtures for metal separations, extraction of platform bio-chemicals from aqueous feeds, and even nanoparticle synthesis.

Conflicts of interest

There are no conflicts to declare.

Acknowledgements

Solvay is kindly acknowledged for providing TOPO and DfE acknowledged for PhD funding (EB).

Notes and references

1 M. A. R. Martins, S. P. Pinho and J. A. P. Coutinho, *J. Solution Chem.*, 2019, **48**, 962–982.
2 Q. Zhang, K. De Oliveira Vigier, S. Royer and F. Jérôme, *Chem. Soc. Rev.*, 2012, **41**, 7108–7146.
3 M. Francisco, A. van den Bruinhorst and M. C. Kroon, *Angew. Chem., Int. Ed.*, 2013, **52**, 3074–3085.
4 E. L. Smith, A. P. Abbott and K. S. Ryder, *Chem. Rev.*, 2014, **114**, 11060–11082.
5 A. P. Abbott, G. Capper, D. L. Davies, R. K. Rasheed and V. Tambyrajah, *Chem. Commun.*, 2003, 70–71.
6 A. P. Abbott, D. Boothby, G. Capper, D. L. Davies and R. Rasheed, *J. Am. Chem. Soc.*, 2004, **126**, 9142–9147.
7 Q. Zeng, Y. Wang, Y. Huang, X. Ding, J. Chen and K. Xu, *Analyst*, 2014, **139**, 2565–2573.
8 I. M. Pateli, K. Binnemans, N. Rodriguez and A. P. Abbott, *RSC Adv.*, 2020, **10**, 28879–28890.
9 M. Gilmore, L. M. Moura, A. H. Turner, M. Swadźba-Kwaśny, S. K. Callear, J. A. McCune, O. A. Scherman and J. D. Holbrey, *J. Chem. Phys.*, 2018, **148**, 193823.
10 C. Florindo, A. J. S. McIntosh, T. Welton, L. C. Branco and I. M. Marrucho, *Phys. Chem. Chem. Phys.*, 2018, **20**, 206–213.
11 C. F. Araujo, J. A. P. Coutinho, M. M. Nolasco, S. F. Parker, P. J. A. Ribeiro-Claro, S. Rudic, B. I. G. Soares and P. D. Vaz, *Phys. Chem. Chem. Phys.*, 2017, **19**, 17998–18009.
12 S. L. Perkins, P. Painter and C. M. Colina, *J. Chem. Eng. Data*, 2014, **59**, 3652–3662.
13 D. V. Wagle, G. A. Baker and E. Mamontov, *J. Phys. Chem. Lett.*, 2015, **6**, 2924–2928.
14 C. R. Ashworth, R. P. Matthews, T. Welton and P. A. Hunt, *Phys. Chem. Chem. Phys.*, 2016, **18**, 18145–18160.
15 O. S. Hammond, D. T. Bowron and K. J. Edler, *Green Chem.*, 2016, **18**, 2736–2744.
16 R. Stefanovic, M. Ludwig, G. B. Webber, R. Atkin and A. J. Page, *Phys. Chem. Chem. Phys.*, 2017, **19**, 3297–3306.
17 D. J. G. P. van Osch, L. F. Zubeir, A. van den Bruinhorst, M. A. A. Rocha and M. C. Kroon, *Green Chem.*, 2015, **17**, 4518–4521.
18 B. D. Ribeiro, C. Florindo, L. C. Iff, M. A. Z. Coelho and I. M. Marrucho, *ACS Sustainable Chem. Eng.*, 2015, **3**, 2469–2477.
19 D. J. G. P. van Osch, D. Parmentier, C. H. J. T. Dietz, A. van den Bruinhorst, R. Tuinier and M. C. Kroon, *Chem. Commun.*, 2016, **52**, 11987–11990.
20 M. J. Kaul, D. Qadah, V. Mandella and M. L. Dietz, *RSC Adv.*, 2019, **9**, 15798–15804.
21 E. E. Tereshatov, M. Y. Boloeva and C. M. Folden III, *Green Chem.*, 2016, **18**, 4616–4622.
22 S. Ruggeri, F. Poletti, C. Zanardi, L. Pigani, B. Zanfrognini, E. Corsi, N. Dossi, M. Salomaki, H. Kivela, J. Lukkari and F. Terzi, *Electrochim. Acta*, 2019, **295**, 124–129.
23 T. E. Phelps, N. Bhawawet, S. S. Jurisson and G. A. Baker, *ACS Sustainable Chem. Eng.*, 2018, **6**, 13656–13661.
24 C. Florindo, L. C. Branco and I. M. Marrucho, *Fluid Phase Equilib.*, 2017, **448**, 135–142.
25 T. Krízek, M. Bursová, R. Horsley, M. Kuchar, P. Tuma, R. Cabala and T. Hlozek, *J. Cleaner Prod.*, 2018, **193**, 391–396.
26 J. Cao, M. Yang, F. Cao, J. Wang and E. Su, *J. Cleaner Prod.*, 2017, **152**, 399–405.
27 J. Cao, L. Chen, M. Li, F. Cao, L. Zhao and E. Su, *Green Chem.*, 2018, **20**, 1879–1886.
28 J. Cao, M. Yang, F. Cao, J. Wang and E. Su, *ACS Sustainable Chem. Eng.*, 2017, **5**, 3270–3278.
29 E. L. P. de Faria, R. S. do Carmo, A. F. M. Cláudio, C. S. R. Freire, M. G. Freire and A. J. D. Silvestre, *Int. J. Mol. Sci.*, 2017, **18**, 2276–2285.
30 Y. P. A. Silva, T. A. P. C. Ferreira, G. Jiao and M. S. Brooks, *J. Food Sci. Technol.*, 2019, **56**, 1649–1654.
31 T. Sato, T. Nakamura and S. Ishikawa, *Solvent Extr. Ion Exch.*, 1984, **2**, 201–212.
32 E. K. Watson and W. A. Rickelton, *Solvent Extr. Ion Exch.*, 1992, **10**, 879–889.
33 P. O. Saboe, L. P. Manker, W. E. Michener, D. J. Peterson, D. G. Brandner, S. P. Deutch, M. Kumar, R. M. Cywar, G. T. Beckham and E. M. Karp, *Green Chem.*, 2018, **20**, 1791–1804.
34 T. Brouwer, M. Blahusiak, K. Babic and B. Schuur, *Sep. Purif. Technol.*, 2017, **185**, 186–195.
35 G. Kim, S. Park and B. Um, *Ind. Crops Prod.*, 2016, **89**, 34–44.
36 S. Uenoyama, T. Hano, M. Hirata and S. Miura, *J. Chem. Technol. Biotechnol.*, 1996, **67**, 260–264.
37 P. Praveen and K. C. Loh, *Chem. Eng. J.*, 2014, **255**, 641–649.
38 P. Praveen and K. Loh, *Chemosphere*, 2016, **153**, 405–413.
39 P. Praveen and K. Loh, *J. Membr. Sci.*, 2013, **437**, 1–6.
40 E. K. Watson, W. A. Rickelton, A. J. Robertson and T. J. Brown, *Solvent Extr. Ion Exch.*, 1988, **6**, 207–220.

41 C. Bayliss and K. Langley, *Nuclear decommissioning, waste management, and environmental site remediation*, Elsevier, 2003.
42 W. Jianchen and S. Chongli, *Solv. Extn. Ion Exch.*, 2001, **19**, 231–242.
43 F. Coleman, G. Srinivasan and M. Swadźba-Kwaśny, *Angew. Chem., Int. Ed.*, 2013, **52**, 12582–12586.
44 J. M. Hogg, L. C. Brown, K. Matuszek, P. Latos, A. Chrobok and M. Swadźba-Kwaśny, *Dalton Trans.*, 2017, **46**, 11561–11574.
45 J. M. Hogg, F. Coleman, A. Ferrer-Ugalde, M. P. Atkins and M. Swadźba-Kwaśny, *Green Chem.*, 2015, **17**, 1831–1841.
46 K. Matuszek, A. Chrobok, J. M. Hogg, F. Coleman and M. Swadźba-Kwaśny, *Green Chem.*, 2015, **17**, 4255–4262.
47 A. van den Bruinhorst, S. Raes, S. A. Maesara, M. C. Kroon, A. C. C. Esteves and J. Meuldijk, *Sep. Purif. Technol.*, 2019, **216**, 147–157.
48 M. Gilmore, É. N. McCourt, F. Connolly, P. Nockemann, M. Swadźba-Kwaśny and J. D. Holbrey, *ACS Sustainable Chem. Eng.*, 2018, **6**, 17323–17332.
49 J. Beare-Rogers, A. Dieffenbacher and J. V. Holm, *Pure Appl. Chem.*, 2001, **73**, 685–744.
50 T. K. Ng and J. G. Zeikus, *Appl. Environ. Microbiol.*, 1986, **52**, 902–904.
51 S. P. Verevkin and C. Schick, *Thermochim. Acta*, 2004, **415**, 35–42.
52 J. A. Bis, P. Vishweshwar, D. Weyna and M. J. Zaworotko, *Mol. Pharming*, 2007, **4**, 401–416.
53 T.-H. Lee, J.-L. Chiou, C.-K. Lee and Y.-H. Kuo, *J. Chin. Chem. Soc.*, 2005, **52**, 833–841.
54 E. Berlinger, F. Berlinger and I. Nelidow, *J. Am. Chem. Soc.*, 1954, **76**, 507–509.
55 K. W. Anderson, T. Ikawa, R. E. Tundel and S. L. Buchwald, *J. Am. Chem. Soc.*, 2006, **128**, 10694–10695.
56 G. A. Olah, G. K. S. Prakash, P. S. Iyer, M. Tashiro and T. Yamato, *J. Org. Chem.*, 1987, **52**, 1881–1884.
57 A. Metzger, S. Bernhardt, G. Manolikakes and P. Knochel, *Angew. Chem., Int. Ed.*, 2010, **49**, 4665–4668.
58 L. J. Reed and C. Niu, *J. Am. Chem. Soc.*, 1955, **77**, 416–419.
59 S. G. Morris, *J. Am. Chem. Soc.*, 1949, **71**, 2056–2057.
60 M. Piattelli, E. Fattorusso, S. Magno and R. A. Nicolaus, *Tetrahedron*, 1963, **19**, 2061–2072.
61 L. M. Fuentes and G. L. Larson, *Tetrahedron Lett.*, 1982, **23**, 271–274.
62 K. Bica and R. D. Rogers, *Chem. Commun.*, 2010, **46**, 1215–1217.
63 W. D. Shrader, J. Celebuski, S. J. Kline and D. Johnson, *Tetrahedron Lett.*, 1988, **29**, 1351–1354.
64 Z. Hou, K. Takamine, O. Aoki, H. Shiraishi, Y. Fujiwara and H. Taniguchi, *J. Org. Chem.*, 1988, **53**, 6077–6084.
65 J. Nicolas, C. Billaud, J. Philippon and A. M. Rouet-Mayer, in *Encyclopedia of Food Sciences and Nutrition*, ed. B. Caballero, Academic Press, 2nd edn, 1982, pp. 678–686.
66 L. Chun-Chen and R. K. Peddinti, *Acc. Chem. Res.*, 2002, **35**, 856–866.
67 R. Dawson and J. M. Nelson, *J. Am. Chem. Soc.*, 1938, **60**, 245–249.
68 D. Magdziak, A. A. Rodriguez, R. W. Van De Water and T. R. R. Pettus, *Org. Lett.*, 2002, **4**, 285–288.
69 P. De La Breteque and M. Beerli, *U.S. Pat.*, 3887681, 1975.
70 E. Uhlemann and W. Mickler, *Anal. Chim. Acta*, 1981, **130**, 177–182.
71 Z. Zhao, Y. Yang, Y. Xiao and Y. Fan, *Hydrometallurgy*, 2012, **125–126**, 115–124.
72 Y. Hasegawa, T. Shimada and M. Niitsu, *J. Inorg. Nucl. Chem.*, 1980, **42**, 1487–1489.
73 I. Mihaylov and P. A. Distin, *Hydrometallurgy*, 1992, **28**, 13–27.
74 D. W. Rackemann, W. O. S. Doherty and T. Crops, *Biofuels, Bioprod. Biorefin.*, 2011, **5**, 198–214.
75 F. D. Pileidis and M. Titirici, *ChemSusChem*, 2016, **9**, 562–582.
76 J. J. Bozell and G. R. Petersen, *Green Chem.*, 2010, **12**, 539–554.
77 O. V. Kotova, S. V. Eliseeva, A. A. Volosnikov, V. A. Oleinikov, L. S. Lepnev, A. G. Vitukhnovskii and N. P. Kuz'mina, *Russ. J. Coord. Chem.*, 2006, **32**, 901–909.
78 V. L. Stanford and S. Vyazovkin, *Ind. Eng. Chem. Res.*, 2017, **56**, 7964–7970.
79 C. N. Hinshelwood, *J. Chem. Soc., Trans.*, 1920, **117**, 156–165.
80 J. Györe and M. Ecet, *J. Therm. Anal.*, 1970, **2**, 397–409.
81 A. M. El-Awad and R. M. Mahfouz, *J. Therm. Anal.*, 1989, **35**, 1413–1421.
82 W. W. Wendlandt and J. A. Hoiberg, *Anal. Chim. Acta*, 1963, **28**, 506–511.
83 S. Gál, T. Meisel and L. Erdey, *J. Therm. Anal.*, 1969, **1**, 159–170.
84 N. R. Rodriguez, A. van den Bruinhorst, L. J. B. M. Kollau, M. C. Kroon and K. Binnemans, *ACS Sustainable Chem. Eng.*, 2019, **7**, 11521–11528.
85 P. G. Blake and G. E. Jackson, *J. Chem. Soc. B*, 1968, 1153–1155.
86 S. C. Moldoveanu, *Pyrolysis of Organic Molecules*, 2019, pp. 483–553.
87 E. Y. Tupikina, M. Bodensteiner, P. M. Tolstoy, G. S. Denisov and I. G. Shenderovich, *J. Phys. Chem. C*, 2018, **122**, 1711–1720.
88 M. Grilc and B. Likozar, *Chem. Eng. J.*, 2017, **330**, 383–397.
89 M. Renz, *Eur. J. Org. Chem.*, 2005, 979–988.
90 J. Gmehling, B. Kolbe, M. Kleiber and J. Rarey, *Chemical Thermodynamics for Process Simulation*, Wiley, New York, 2012.
91 J. A. P. Coutinho, S. I. Andersen and E. H. Stenby, *Fluid Phase Equilib.*, 1995, **103**, 23–39.
92 J. Nývlt, *Solid-Liquid Phase Equilibria*, Elsevier Scientific Pub. Co., Amsterdam, 1977.
93 G. J. Maximo, M. C. Costa and A. J. A. Meirelles, *Phys. Chem. Chem. Phys.*, 2014, **16**, 16740–16754.
94 B. Predel, M. Hoch and M. J. Pool, *Phase Diagrams and Heterogeneous Equilibria*, Springer-Verlag Berlin Heidelberg, 2004, pp. 17–87.
95 J. Kříž, J. Dybal, E. Makrlík, J. Budka and P. Vaňura, *J. Phys. Chem. A*, 2009, **113**, 5896–5905.
96 U. Mayer, V. Gutmann and W. Gerger, *Monatsh. Chem.*, 1975, **106**, 1235–1257.
97 M. A. Beckett, G. C. Strickland, J. R. Holland and S. Varma, *Polymer*, 1996, **37**, 4629–4631.

98 K. M. Diemoz and A. K. Franz, *J. Org. Chem.*, 2019, **84**, 1126–1138.
99 K. A. Al-Farhan, *Acta Crystallogr.*, 2003, **C59**, 179–180.
100 K. A. Al-Farhan, *Acta Crystallogr.*, 2004, **C60**, 531–532.
101 D. B. Chesnut and A. Savin, *J. Am. Chem. Soc.*, 1999, **121**, 2335–2336.
102 K. A. Lyssenko, G. V. Grintselev-Knyazev and M. Y. Antipin, *Mendeleev Commun.*, 2002, **12**, 128–130.
103 H. Guerrero, C. Lafuente, F. Royo, L. Lomba and B. Giner, *Energy Fuels*, 2011, **25**, 3009–3013.
104 G. Ghersini, in *Extraction Chromatography*, ed. T. Braun and G. Ghersini, Elsevier, 1975, pp. 68–133.
105 J. M. Warden and C. J. King, *J. Chem. Eng. Data*, 1978, **23**, 144–148.
106 P. Myrdal, G. H. Ward, R. M. Dannenfelser, D. Mishra and S. H. Yalkowsky, *Chemosphere*, 1992, **24**, 1047–1061.
107 E. Chemical Agency, ECHA, Regist. Subst. Doss.
108 B. Gupta, N. Mudhar, Z. Begum and I. Singh, *Hydrometallurgy*, 2007, **87**, 18–26.
109 A. K. De and U. S. Ray, *Sep. Sci.*, 1972, **7**, 409–417.
110 T. Katsura and H. Abe, *U.S. Pat.*, 3920450, 1975.
111 L. A. Woodward and A. A. Nord, *J. Chem. Soc.*, 1956, 3721–3722.
112 P. F. M. van Gaans, H. A. J. Oonk and G. Somsen, *J. Solution Chem.*, 1990, **19**, 831–854.
113 X. Lu, L. Wang, X. Wang and X. Niu, *Nonferrous Mater.*, 2008, **60**, 105–108.
114 B. Das, R. N. Roy, K. S. Pitzer, D. R. Gregory and S. A. Kiefer, *J. Solution Chem.*, 2000, **29**, 289–297.